ELECTROMAGNETIC CALORIMETRY AND SPECTROSCOPY

Juliet Lee- Franzini

Lab Nazionali Frascati

Karlsruhe University

Karlsruhe - 2003

OUTLINE

PRINCIPLE of EM CALORIMETERS

HOMOGENEOUS CALORIMETERS

CUSB-I, CUSB-II

Upsilon Spectroscopy

χ_b Fine Stucture

Color Magnetic transitions

Search for Exotica

A SAMPLING CALORIMETER: KLOE

Light Quark Spectroscopy

this
is
tex

WHAT IS A CALORIMETER?

It is a device which measures the energy of an incident (absorbed) particle.

As described previously in lecture two by Paolo, electrons and photons with more than a few MeV develop an electromagnetic shower as they traverse matter.

Determines both the initial energy, and entry position (the direction if the production point is known).

The calorimeters may be homogeneous, or made of active and passive layers so that the energy deposits are sampled at different depth along the shower development.

Electromagnetic cascade

At high energy both radiation and pair-production will happen repeatedly in cascade. It makes little difference whether it all started with an electron or a photon. As the cascade develops the number of particles and photons increases. Charged particles loose energy to the medium, the beginning a signal of the shower. At some point the energy of photon and electrons becomes low enough that radiation and pair production stop.

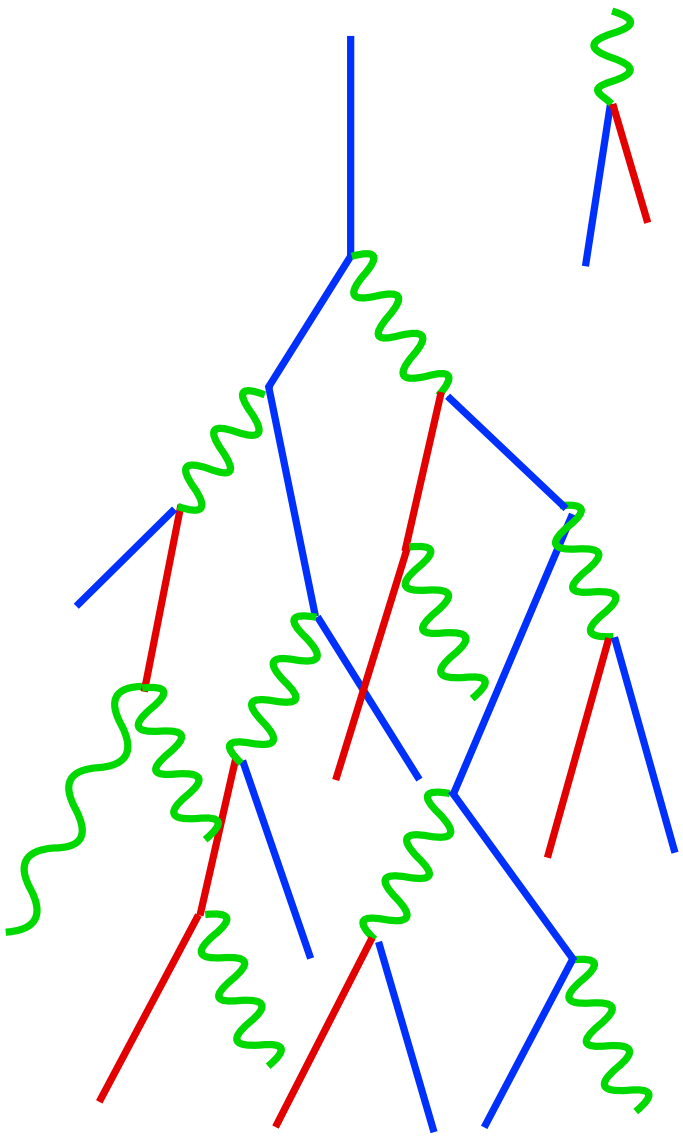

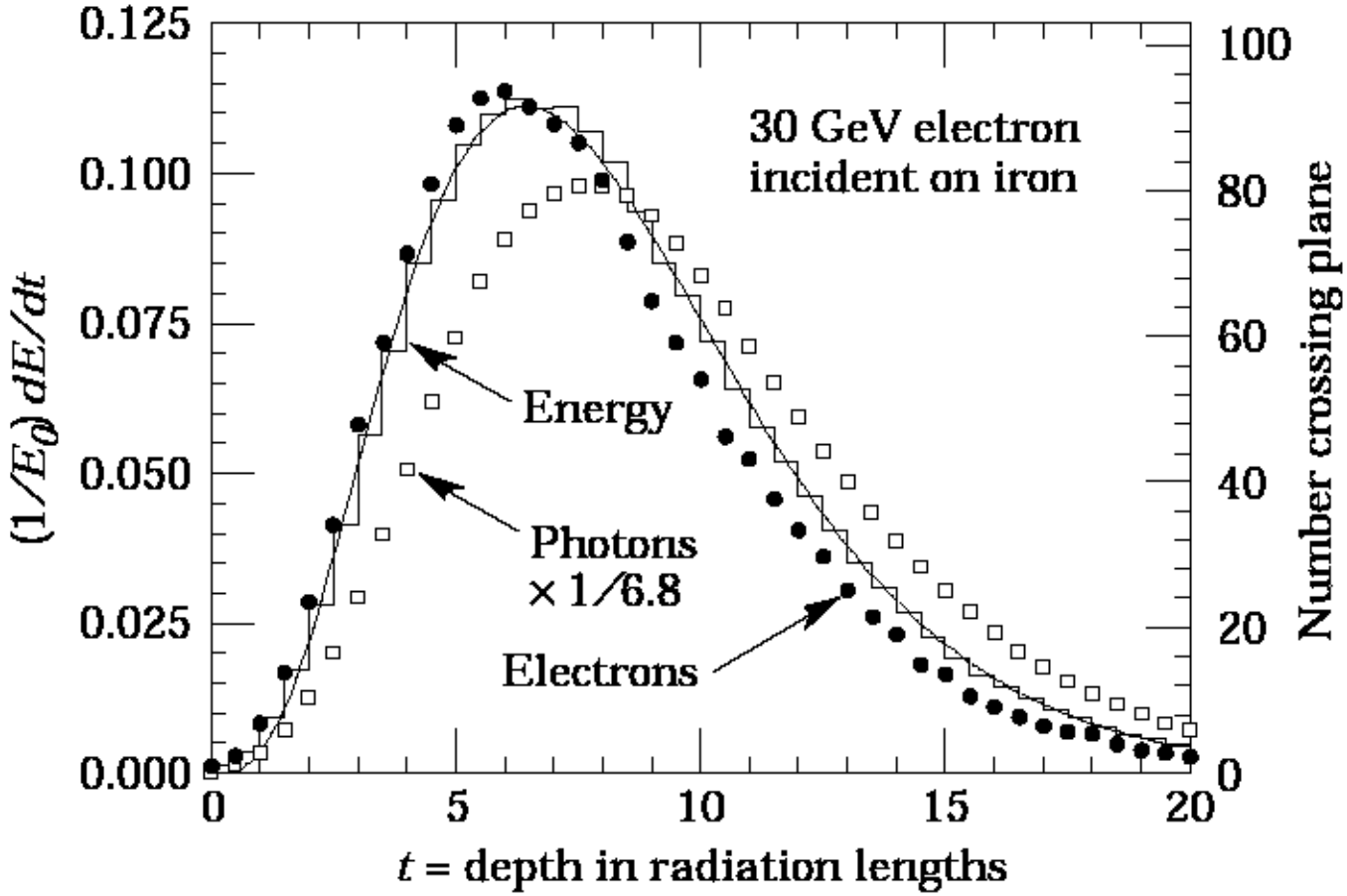

Shower profiles for fractional energy loss and number of particles.

Detection of the number of particles or the energy measures the photon (or electron or positron) energy.

EM shower developing in the plates in a Wilson Chamber.

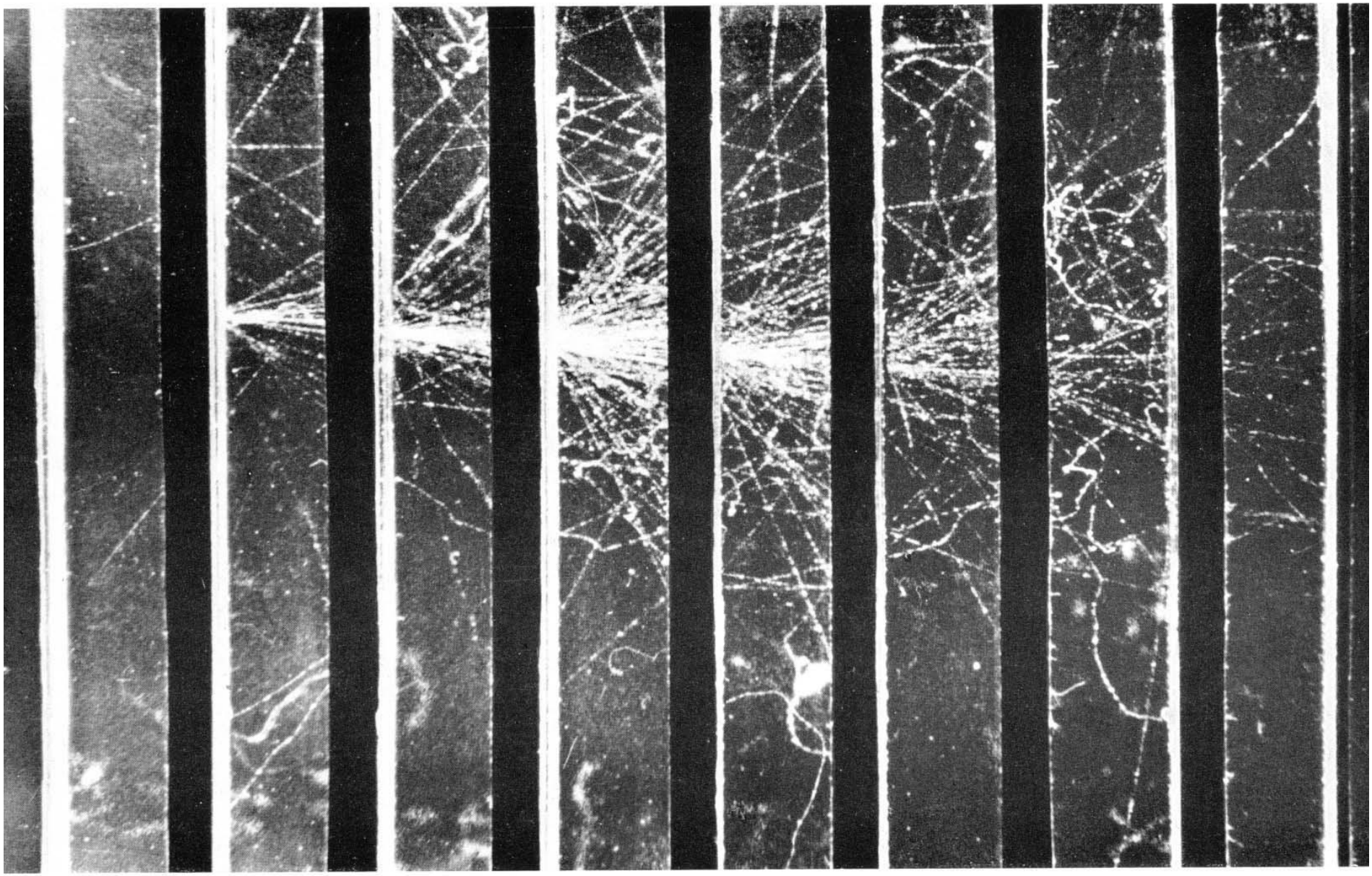

HOMOGENEOUS CALORIMETERS

By homogeneous we mean that the whole detector is made of the same active material, inorganic scintillators, usually NaI, BGO or CsI crystals.

In order to measure the energy contained in the shower, the calorimeter is composed ideally of truncated pyramidal crystals whose apex points to the interaction region.

Since the shower may not be contained within one crystal, one has to add the energy depositions from adjacent towers as well.

WHY and WHICH CRYSTALS TO USE?

Since the first days of gamma spectroscopy, NaI has been the favorite because of its high light yield and easy availability (in small sizes).

Its draw backs are that it is extremely hygroscopic, mechanically fragile and expensive at large sizes. Therefore whenever large areas need to be covered and with less demanding characteristics, high energy experimenters made do with lead glass blocks which however gives much less light output.

Two other inorganic crystals have in the last decades been employed in calorimeters, BGO first by us, then L3, much later CsI by CLEO, then Babar and BELLE.

Properties of BGO, NaI and CsI Crystals

Material	BGO	NaI	CsI
Density, g/cm^3	7.1	3.67	4.53
Radiation Length [cm]	1.12	2.59	1.85
Nuclear interaction length [cm]	22.0	41.4	36.5
Molière radius [cm]	2.7	4.3	3.8
Photons/keV	5-10	40	10-20
Temp. coefficient, %/°C	-1	-0.4	-0.5
Cost, \$/cm^3	15-20	1-2	3(?)

Longitudinal Segmentation

However, electrons, photons and hadrons have different shower development characteristics, thus one would like to measure the energy deposition profile. Hence one needs to have longitudinal segmentation to measure the shower development at different depth.

But how to place photomultipliers to read out light from the crystals to have information in both directions and still have a hermetic detector?

The solution has been, in low multiplicity situations, to insert thin position sensors such as chambers, silicon detectors, in between the crystal layers.

The CUSB-I NAI-Pb Glass Calorimeter

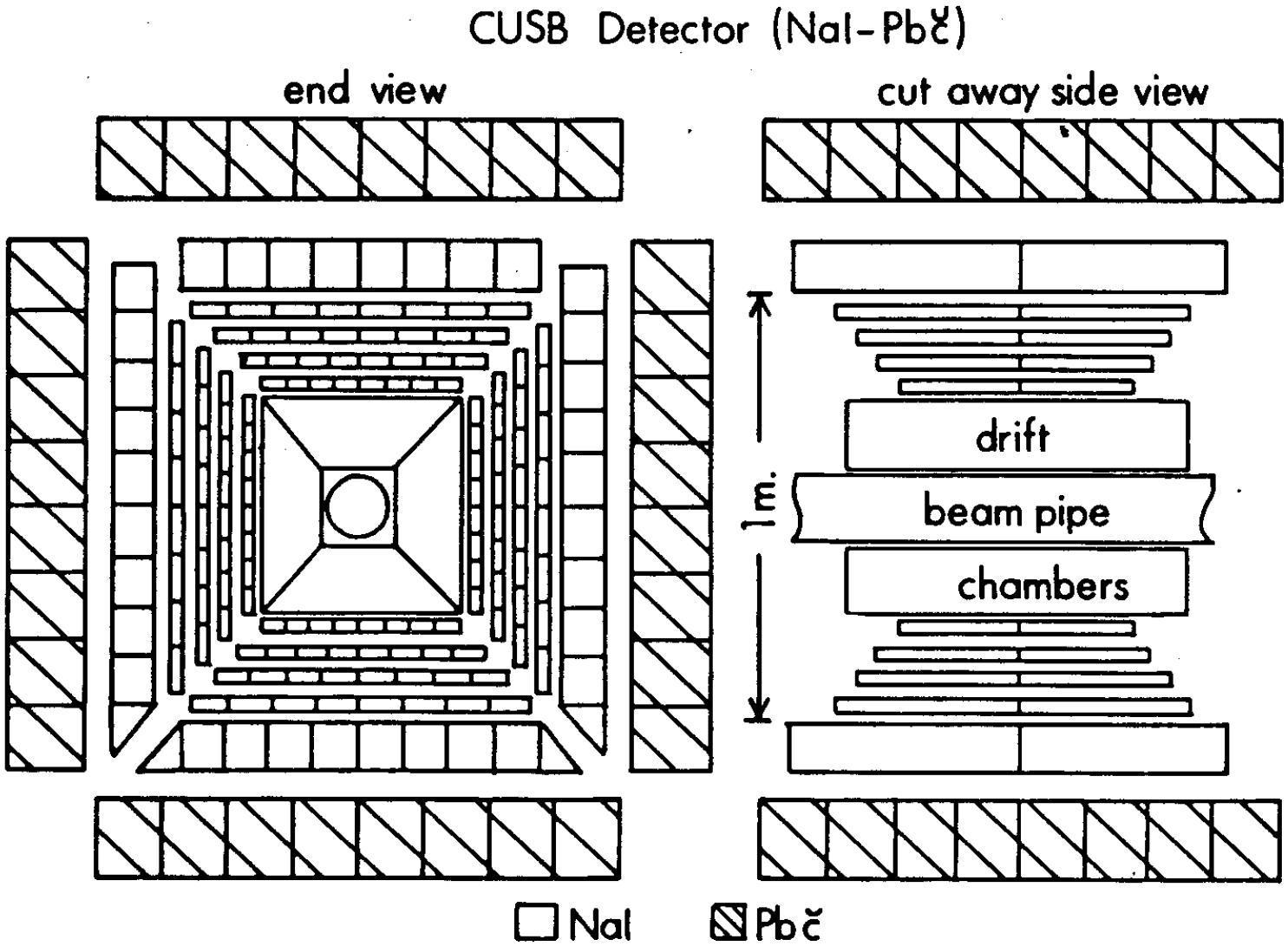

As illustrated in the previous figure, the CUSB-I spectrometer is composed of four quadrant of 5 layers of hermetically sealed NaI crystals, 2.86cm thick (1st 4 layers, 5th 10.4cm), width graduating from 5.78 to 10.4cm, and length from 27 to 50.6cm. It is, normal incidence 8.3 X_0 thick.

Between the five layers there are four planes of multi-wire proportional chambers with cathode strip read out to provide position measurements of shower centroids and minimum ionizing particles.

Each NaI array quadrant is backed up by an array of 8×8 Pb glass total absorption Cherenkov counters, each block of dimension 15.0×15.0×17.5cm^3. Their thickness corresponds to 7.7 X_0, thus between the NaI and Pb glass the spectrometer is 16 X_0 thick.

Inside the NaI array, there is a set of small drift chambers to provide tracking of charged particles. Surrounding the calorimeter is a system of scintillation counters, they are located behind about two nuclear interaction lengths, thus detect penetrating particles, muons.

In the next two figures we show the energy deposition patterns in the calorimeter from (1) A Bhabha scattering event $e^+ + e^- \rightarrow e^+ + e^-$ at the CESR e^+e^- collider at about 10 GeV,

(2) An Υ hadronic decay event. Note the minimum ionizing particles can be easily recognized from their constant energy deposition per X_0.

Bhabha Scattering Event in CUSB-I at CESR

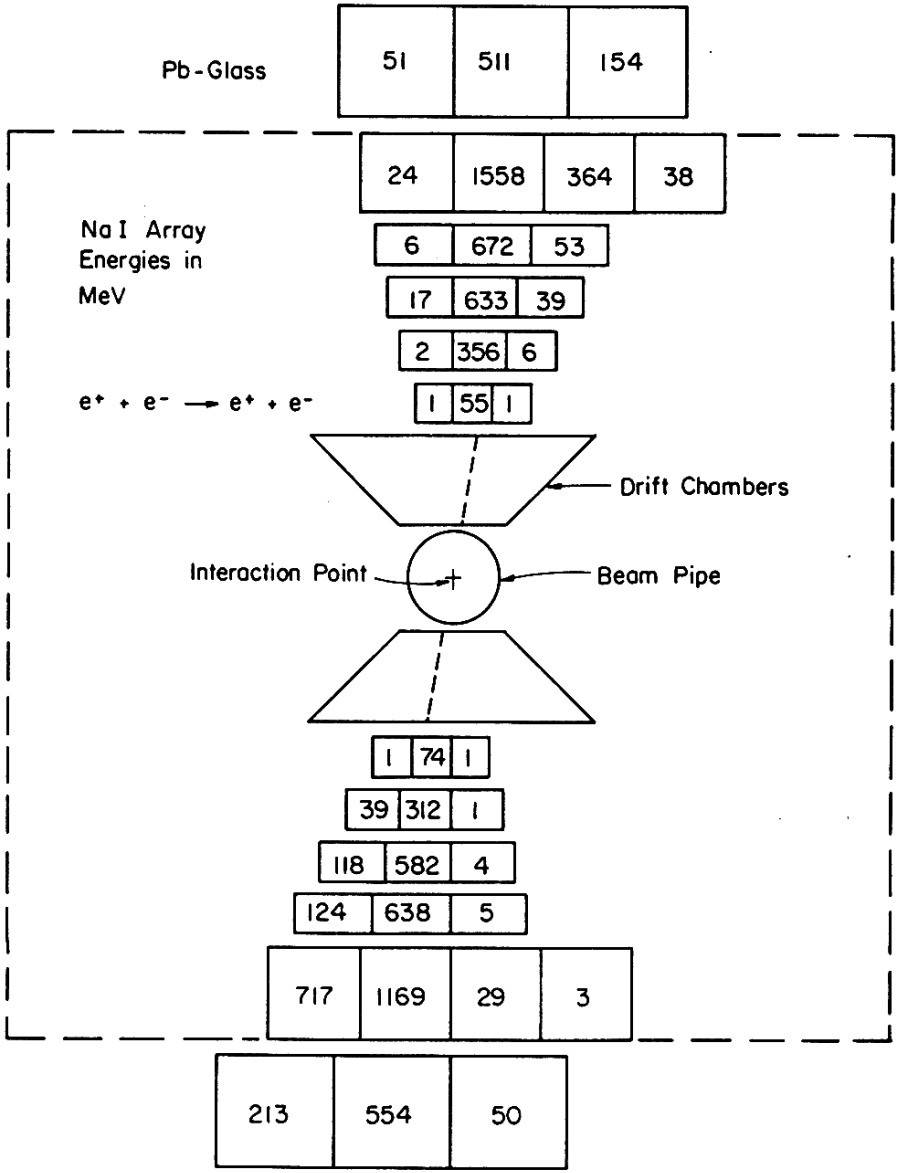

Upsilon Hadronic Decay Event in CUSB-I at CESR

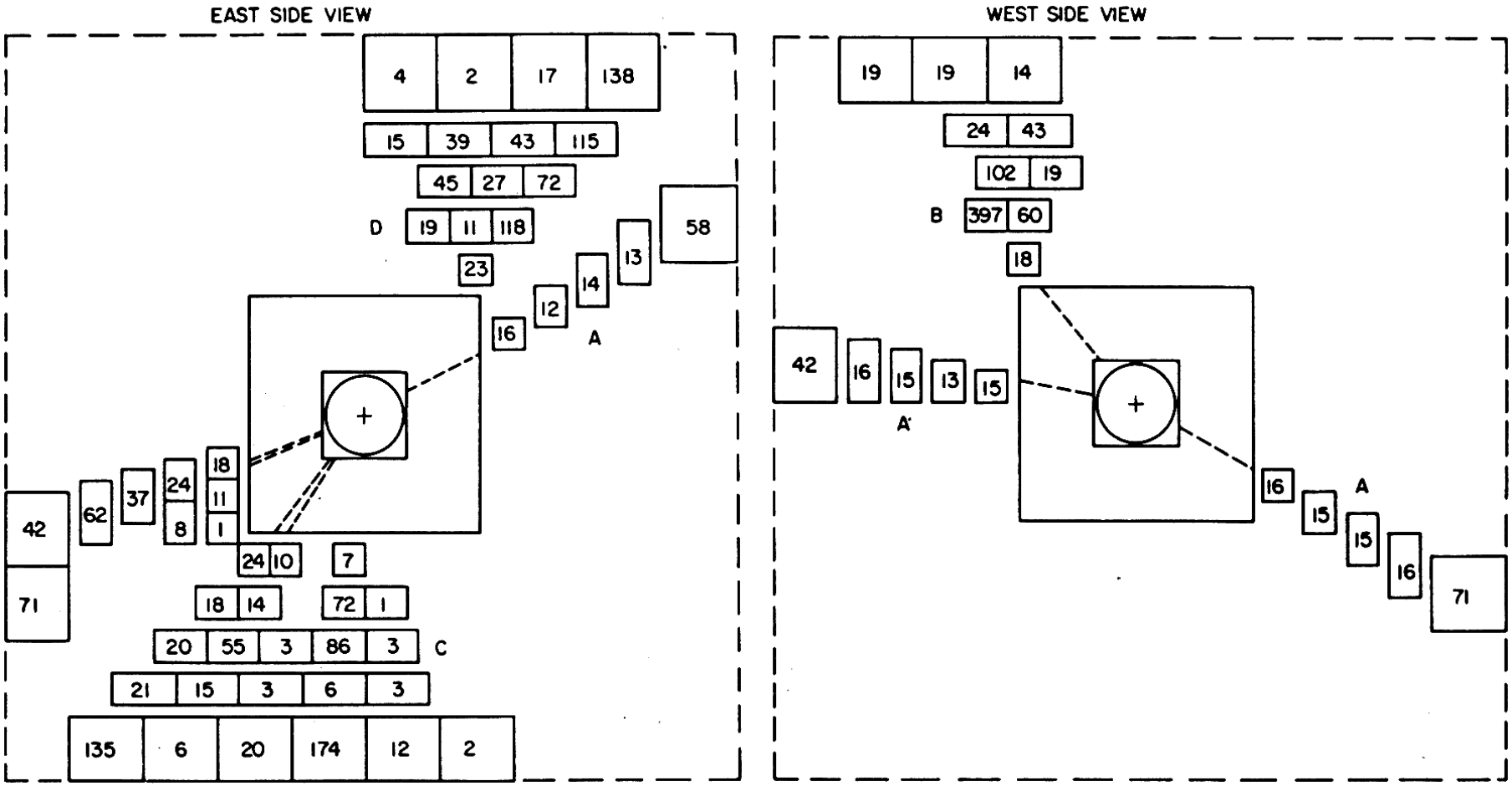

Upsilon Spectroscopy

The Υ system was discovered at Fermilab in 1977 from seeing an enhancement in dimuon production from 400 GeV proton nucleus collisions.

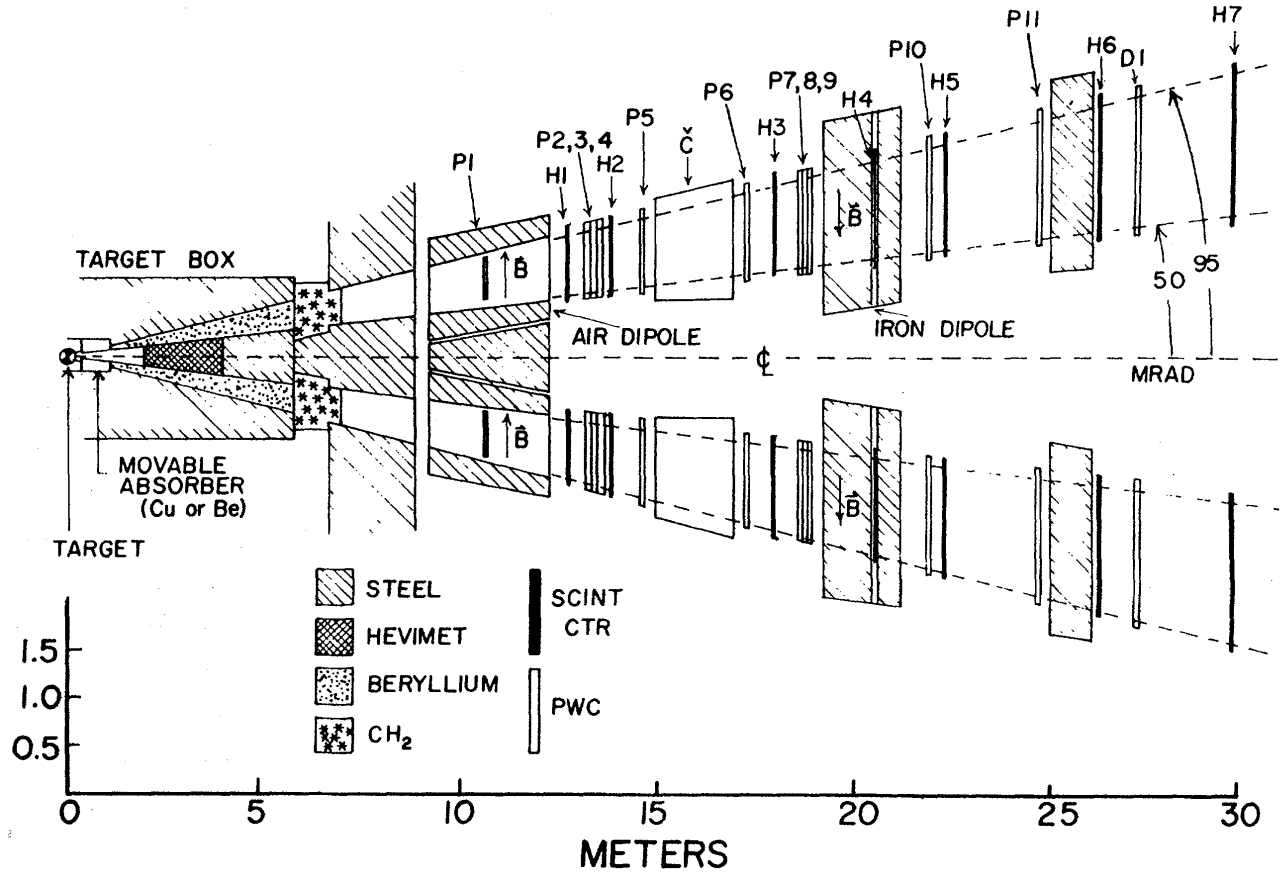

Dimuon production as function of the invariant mass of the dimuon pair.
Note the huge continuum background, known as the DRELL-YAN process, which has to be subtracted.

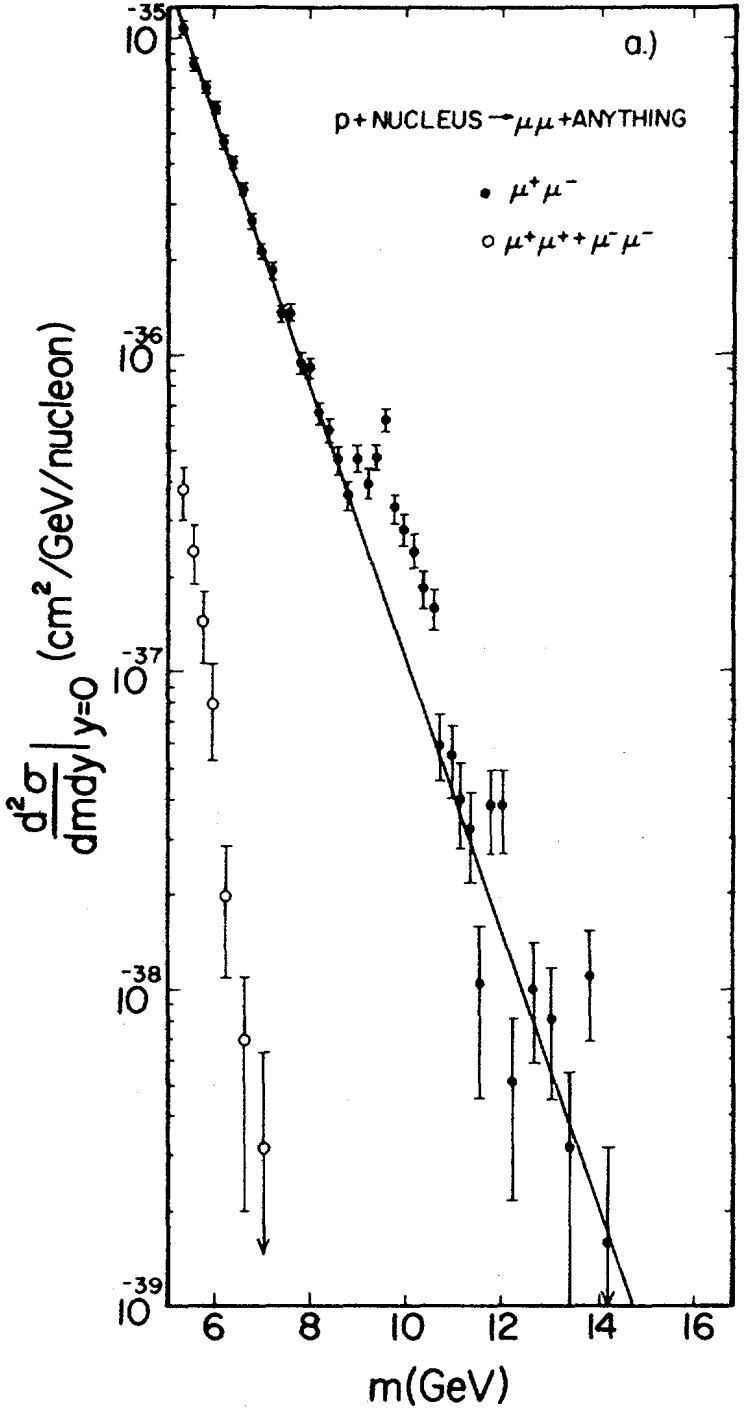

Signal after background subtraction.

Much more solid and displaced from OOPS-Leon.

Enhancement interpreted as a group of unresolved $Q\bar{Q}$ bound states.

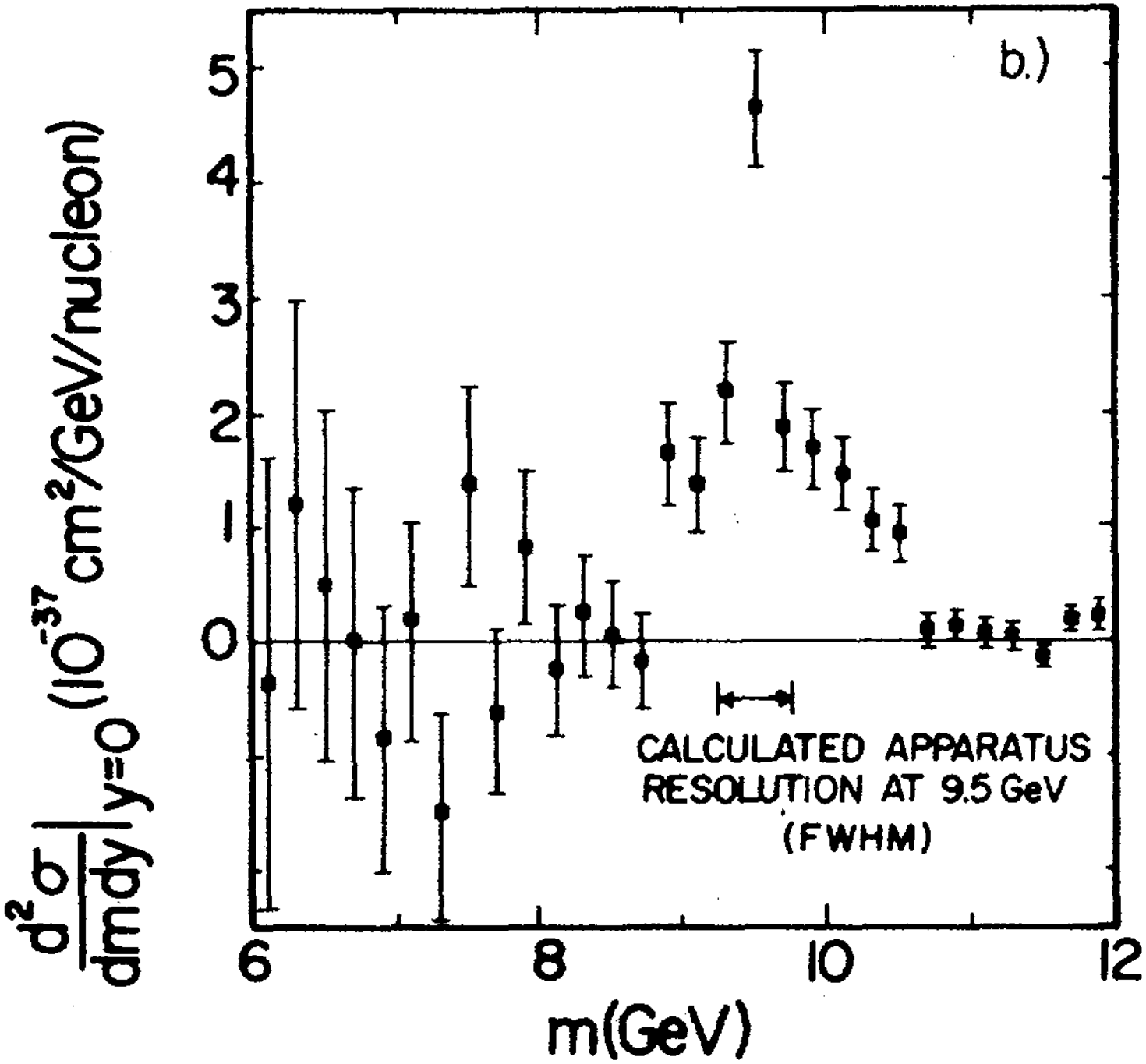

Upsilon Production At e^+e^- Colliders.

At a Collider, when the total beam energy is equal to $M_V/2$ where V is a vector meson with the same quantum numbers as the virtual photon, $J^{PC} = 1^{--}$, the production cross section is:

$$\sigma(e^+e^- \to hadrons)$$

$$= \frac{6\pi^2}{M_V^2} \frac{\Gamma_{ee}\Gamma_{had}}{(E_{cm} - M_V^2)^2 + \Gamma_{tot}^2/4}$$

and defining

$$\Gamma_{tot} = \frac{\Gamma_{ee}}{B_{\mu\mu}}$$

we find

$$A = \frac{6\pi^2}{M_V^2} \frac{\Gamma_{ee}\Gamma_{had}}{\Gamma_{tot}} \epsilon_{rad},$$

which for $Q\bar{Q}$ states is a resonance much wider than the instru-

mental resolution. Assuming lepton universality

$$\frac{\Gamma_{had}}{\Gamma_{tot}} = 1 - 3B_{\mu\mu}$$

Then the Leptonic width is

$$\Gamma_{ee} = \frac{AM_V^2}{6\pi^2}\frac{1}{(1-3B_{\mu\mu})}$$

The Upsilons have very narrow total and leptonic widths, for ex. those of the Υ ground state are about 50 keV and 1 keV respectively. Both are obtained from measurements of the cross section and $B_{\mu\mu}$.

The level spacings of bound states of $Q\bar{Q}$ systems are typically less than 600 MeV, which means the kinetic energies of the bound quarks are small compared to the quark masses.

This means the non-relativistic Schroedinger's equation, assuming a binding potential V, can be used to predict the energy spacings of the $^3S_1$ states.

$$H\Psi = E\Psi$$

$$H = 2m_Q^2 + p^2/m_Q + V(r) + const$$

Several potentials were proposed:

(1) The Cornell Potential

$$V(r) = -\frac{4}{3}\frac{\alpha_s}{r} \qquad \text{for } r \ll \frac{1}{\Lambda}$$

where Λ is the QCD scale parameter and α_s the QCD coupling

constant.

$$V(r) = kr, \qquad \text{for } r \gg \Lambda$$

where k is the string constant.

$$V(r) = -\frac{4}{3}\frac{\alpha_s}{r} + kr$$

(2) The Richardson-Buchmuller Potential:

$$V(q^2) = -\frac{4}{3}\frac{12\pi}{(33-2n_f)}\frac{1}{q^2\ ln(1+\frac{q^2}{\Lambda^2})}$$

(3) Purely empirical potentials,

$$V(r) = 5.82GeV\left(\frac{r}{GeV^{-1}}\right)^{0.104}$$

(4) Purely logarithmic potentials

$$V(r) = 0.7GeV\ ln(\frac{r}{2GeV})$$

How Upsilon states Annihilate and Decay

The ground state Υ can only annihilate either to 3 gluons (+ γgg) or back through a virtual photon to lepton, quark pairs:

$$\Gamma_{ee} = \Gamma_{\mu\mu} = \Gamma_{\tau\tau}$$

$$= \frac{16\alpha^2 e_Q^2}{M_V^2}|\psi(0)|^2(1 - \frac{16\alpha_s}{3\pi})$$

$$\Gamma_{q\bar{q}} = 3\sum e_{q_i}^2 \Gamma_{ee} = R\Gamma_{ee}$$

$$\Gamma_{ggg} = \frac{40}{81}\alpha_s^3 \ \frac{(\pi^2 - 9)}{\pi} \ \frac{|\psi(0)|^2}{m_Q^2}\left(1 - 4.9\frac{\alpha_s}{\pi}\right)$$

$$\frac{\Gamma_{\gamma gg}}{\Gamma_{ggg}} = \frac{45}{9}\frac{\alpha}{\alpha_s}e_Q^2.$$

this is tex

The Υ states thus enables us to measure α_s very precisely, the results were quoted in Christine Davies's lecture and compared favorably with her Lattice QCD calculations.

Resonance	$B_{\mu\mu}$ (%)	Γ (keV)	$\alpha_s(m_b)$
Υ(1S)	2.61±0.09	51.1±3.2	0.174±0.004
Υ(2S)	1.38±0.25	42.3±9.2	0.176±0.016
Υ(3S)	1.73±0.15	27.7±3.7	0.173±0.008
Average	—	—	0.1736±0.0033±0.017

Υ Annihilation Diagrams (top)

$\Upsilon(4S)$ Decaying into B-mesons (bottom)

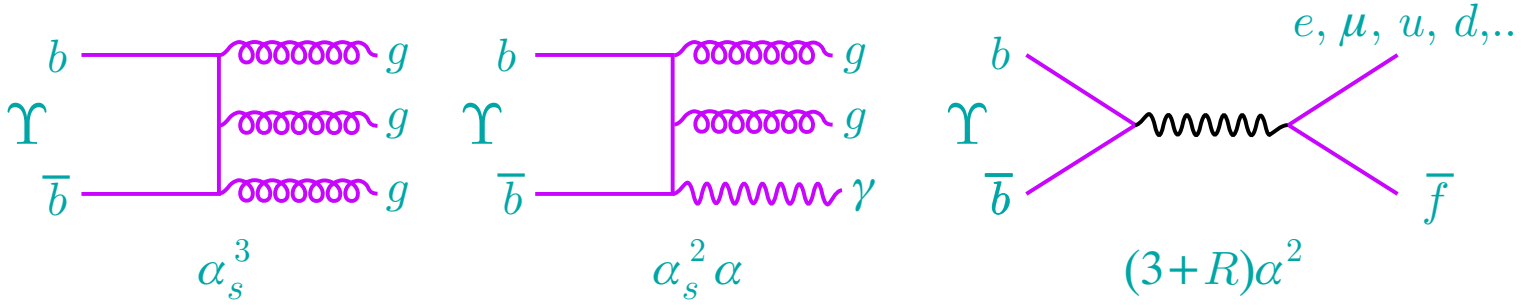

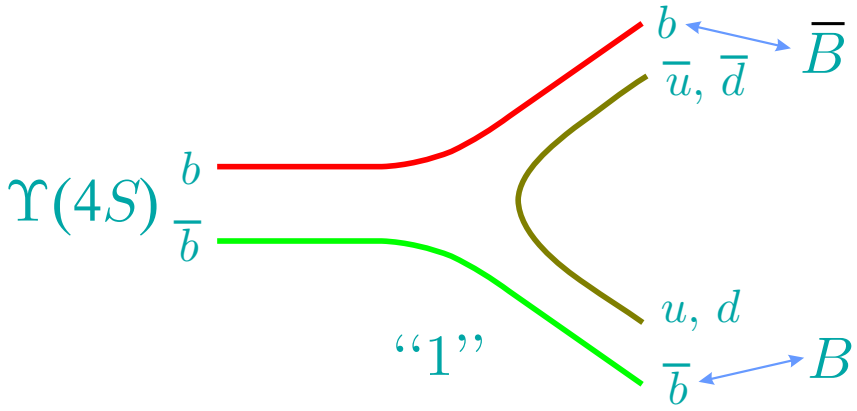

The higher Υ levels (more massive), in addition to annihilations, can reach P states(and back to lower Υ levels) via electromagnetic transitions, and to the lower Υ states via $\pi\pi$ transitions.

Electromagnetic Transitions Rates

$$\Gamma_{E1}(n^3S_1 \to \gamma\ n'^3P_{J_f}) = \frac{4\alpha e_Q^2 E_\gamma^3}{27}(2J_f+1)\langle r\rangle^2$$

$$\Gamma_{E1}(n^3P_J \to \gamma\ n'^3S_1) = \frac{4\alpha e_Q^2 E_\gamma^3}{27}\langle r\rangle^2$$

where

$$\langle r\rangle = \langle \Psi_{n'L'}|r|\Psi_{nL}\rangle.$$

Amplitudes for :(a) electric dipole transitions (E1) ${}^3S({}^3P) \rightarrow {}^3P({}^3S) + \gamma$

(b) double color-electric dipole transitions $n^3S \rightarrow (n-1)^3 + gg(2\pi)$.

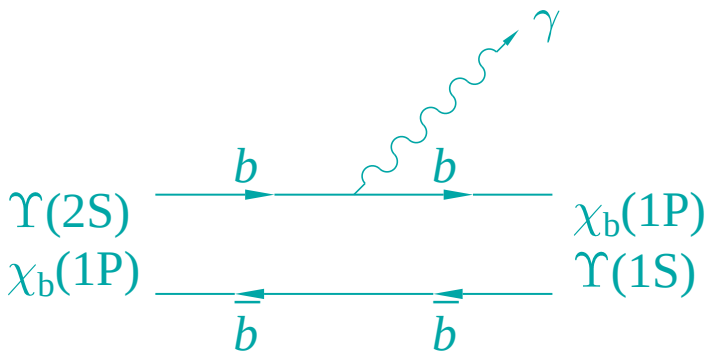

(a)

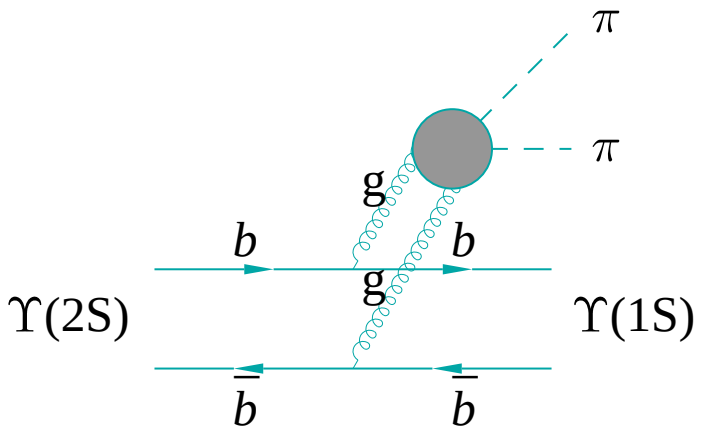

(b)

The October 18th, 1979 configuration of CUSB-0

this
is
tex

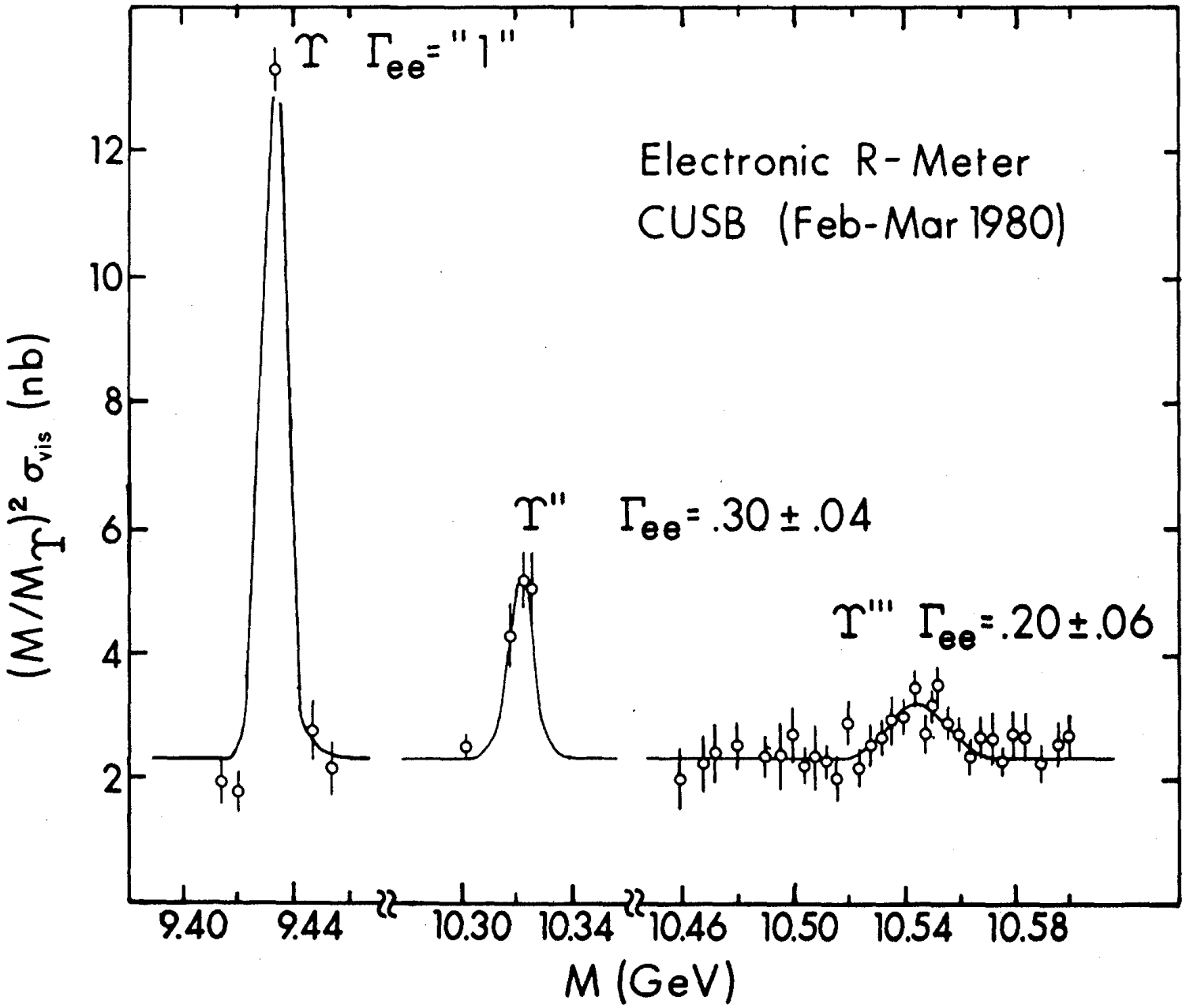
Υ Γee="1"
Electronic R-Meter
CUSB (Feb-Mar 1980)
Υ'' Γee=.30±.04
Υ''' Γee=.20±.06
(M/MΥ)² σvis (nb)
12
10
8
6
4
2
9.40
9.44
10.30
10.34
10.46
10.50
10.54
10.58
M (GeV)

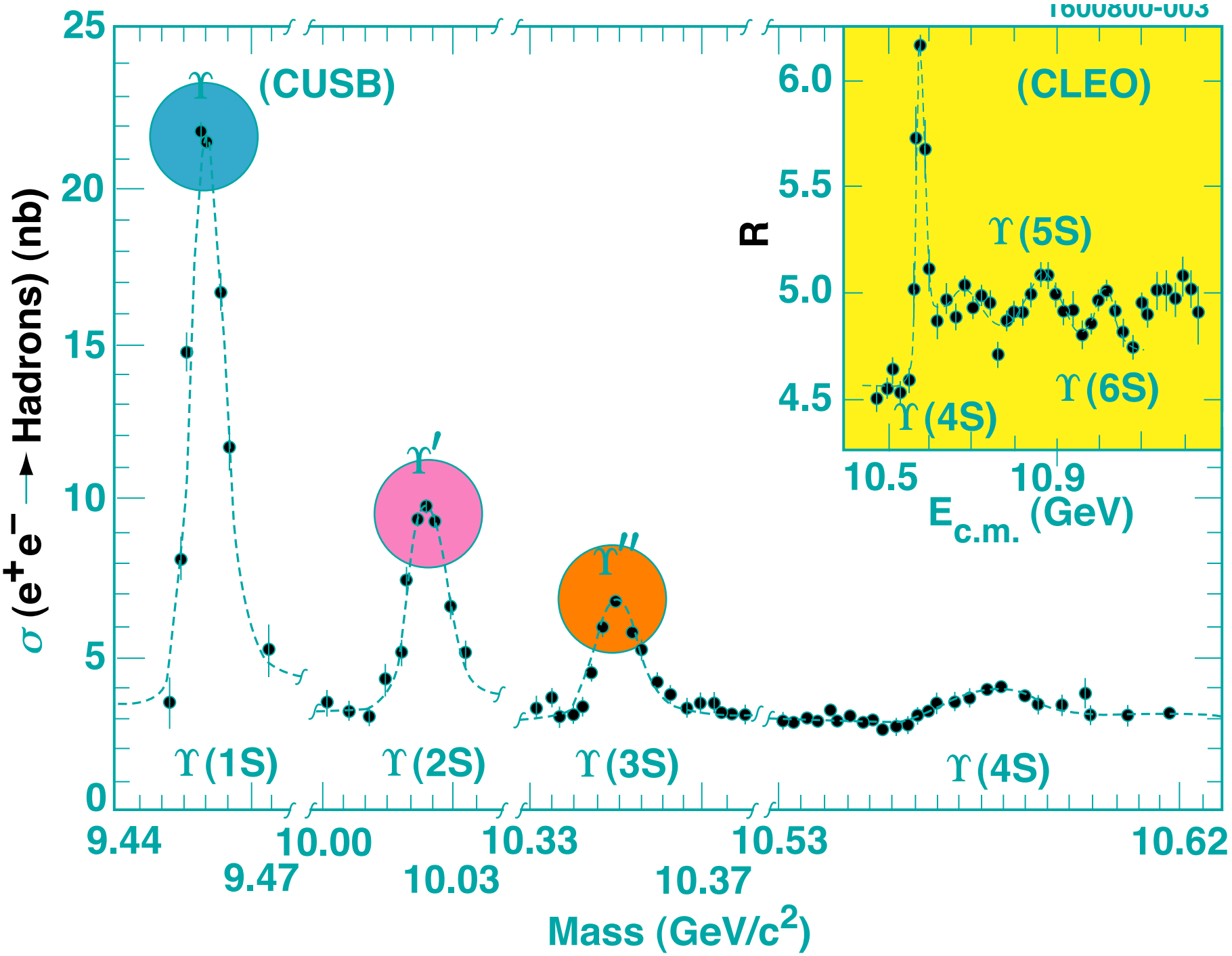
1600800-003
(CUSB)
(CLEO)
Υ(5S)
Υ(6S)
Υ(4S)
R
6.0
5.5
5.0
4.5
10.5
10.9
E c.m. (GeV)
σ (e+e− → Hadrons) (nb)
25
20
15
10
5
0
Υ
Υ′
Υ″
Υ(1S)
Υ(2S)
Υ(3S)
Υ(4S)
9.44
9.47
10.00
10.03
10.33
10.37
10.53
10.62
Mass (GeV/c2)

r dependence of $Q\bar{Q}$ potentials

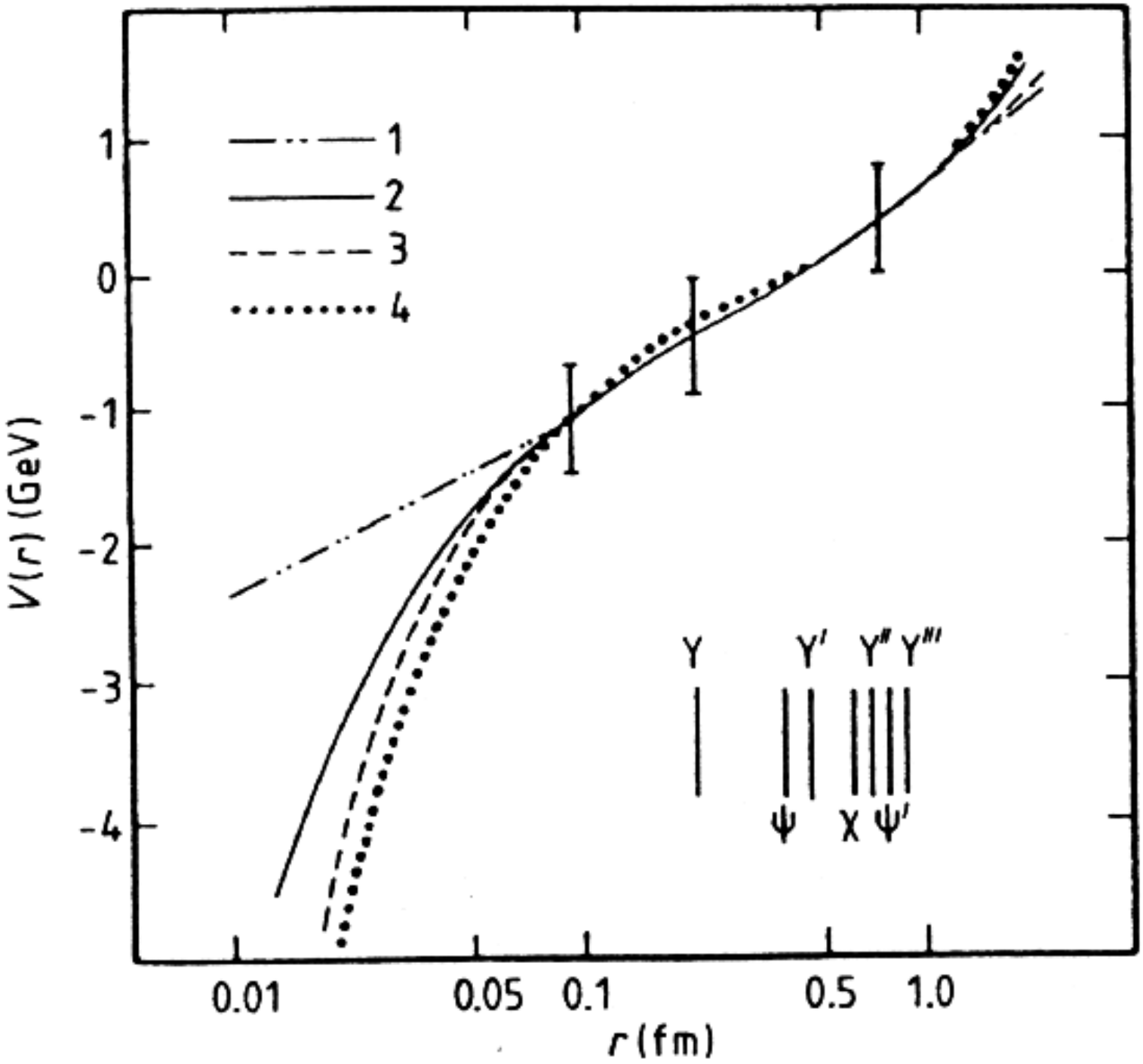

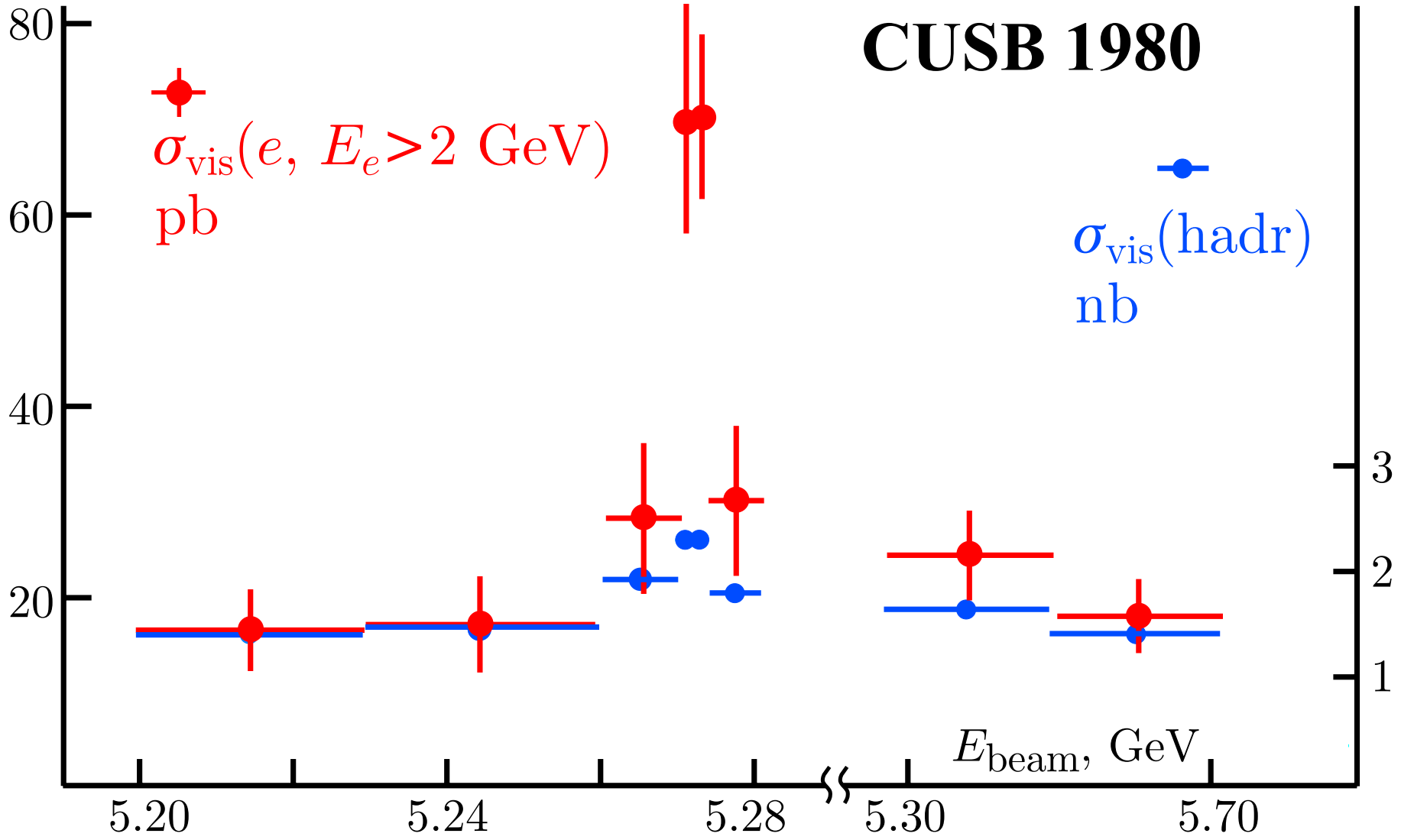
CUSB 1980
$\sigma_{\rm vis}(e,\ E_e{>}2$ GeV)
pb
$\sigma_{\rm vis}$(hadr)
nb
80
60
40
20
3
2
1
$E_{\rm beam}$, GeV
5.20
5.24
5.28
5.30
5.70

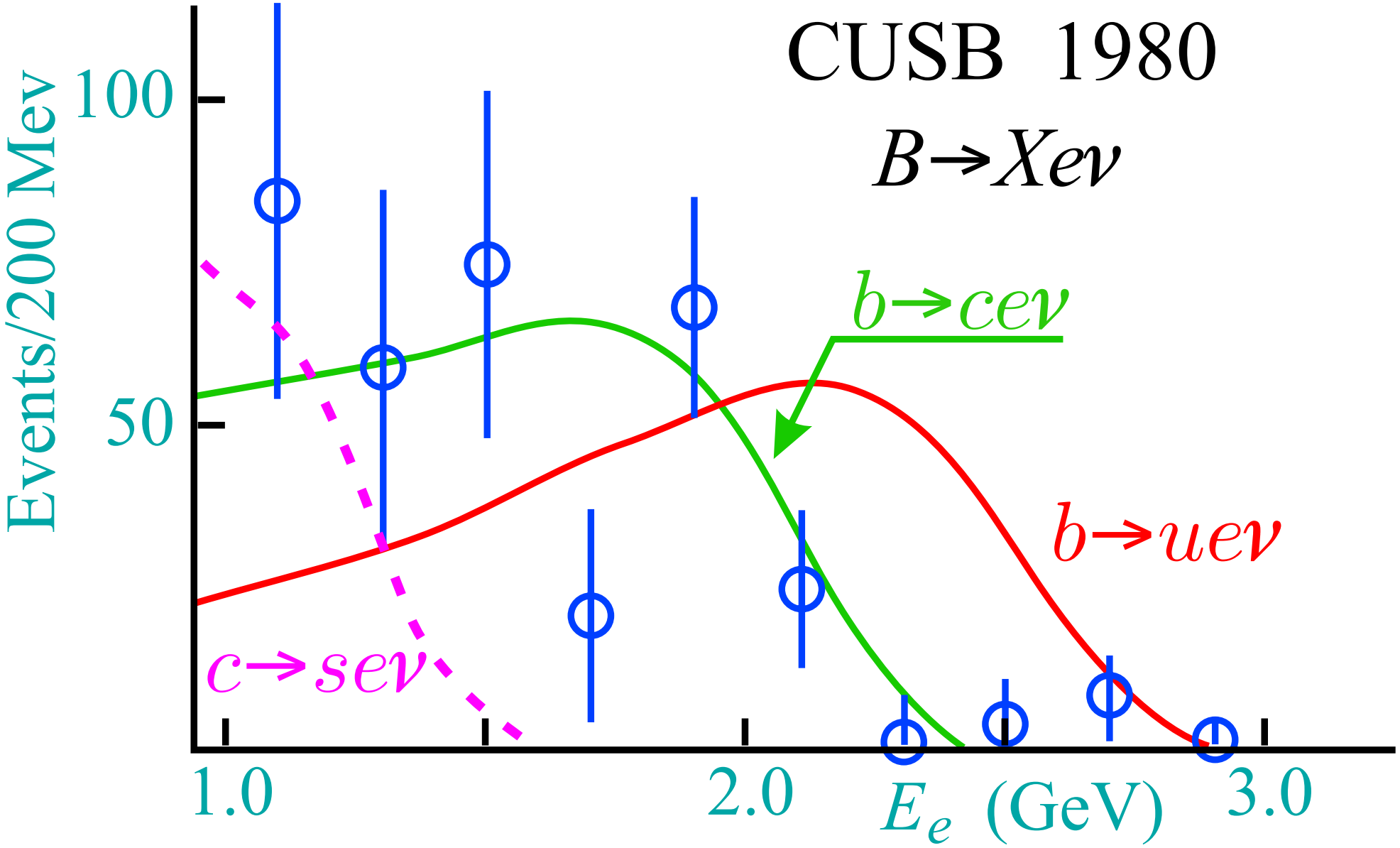
CUSB 1980
$B \to Xe\nu$
Events/200 Mev
100
50
$b \to ce\nu$
$b \to ue\nu$
$c \to se\nu$
1.0
2.0
3.0
E_e (GeV)

In 1984, we decided to upgrade CUSB-I for improved resolution se we could refine our $b\bar{b}$ spectroscopy study.

Given the space constraints, we decided to squeeze down everything. The beam pipe was reduced by $\times 3$ and the drift chamber, constructed directly on it, was also reduced by $\times 3$.

In the vacated space we inserted a calorimeter of 11.6 X_0!!!

It consists of 360 BGO crystals forming 5 concentric cylinders about 22mm thick.

Silicon pads (reverse biased surface barrier silicon detectors) are placed between the first and second layer of BGO to measure the θ-coordinate of shower centroids.

Two plastic scintillator end caps increase the solid angle for two nearly collinear leptons from Υ decays.

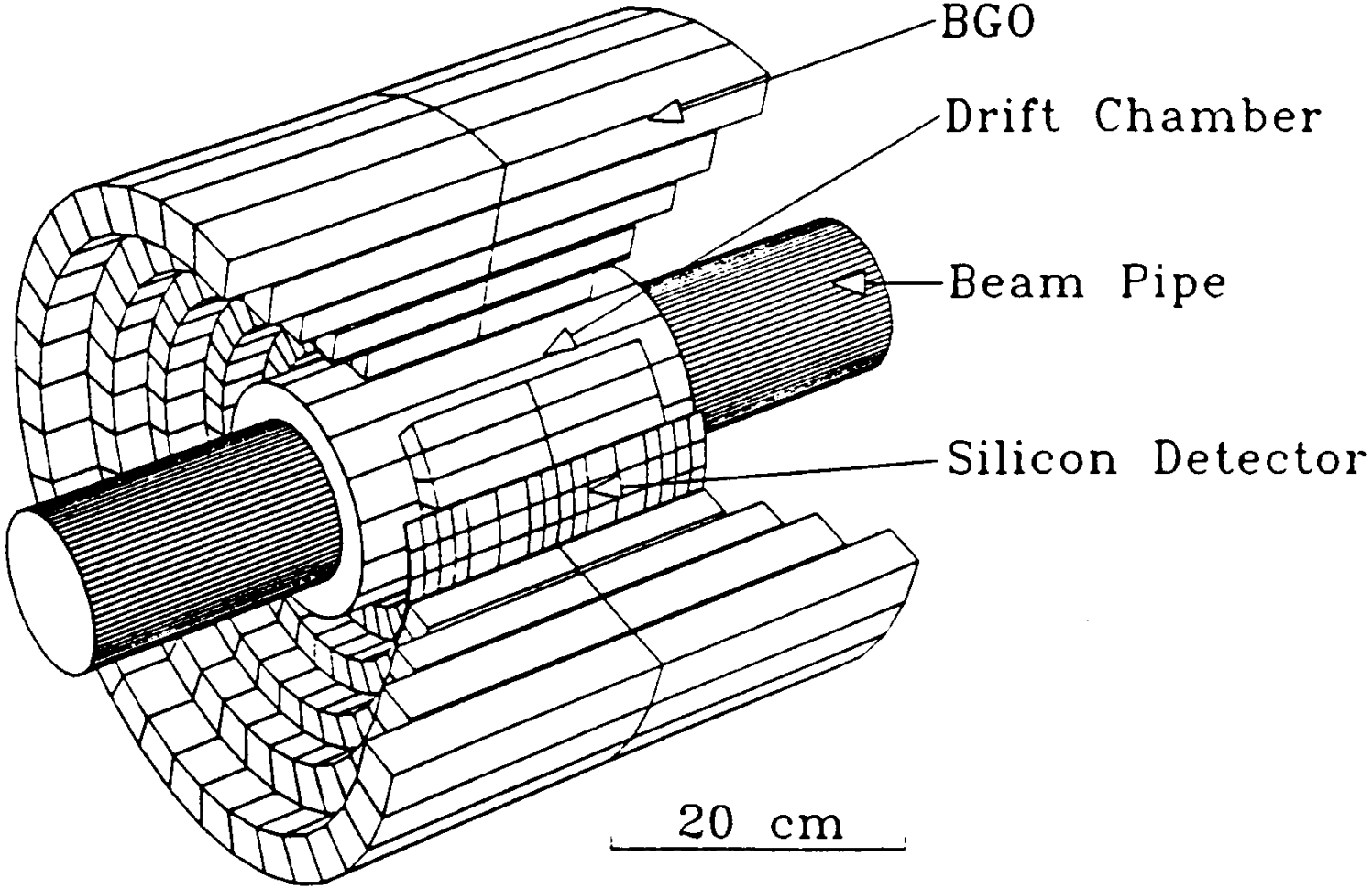

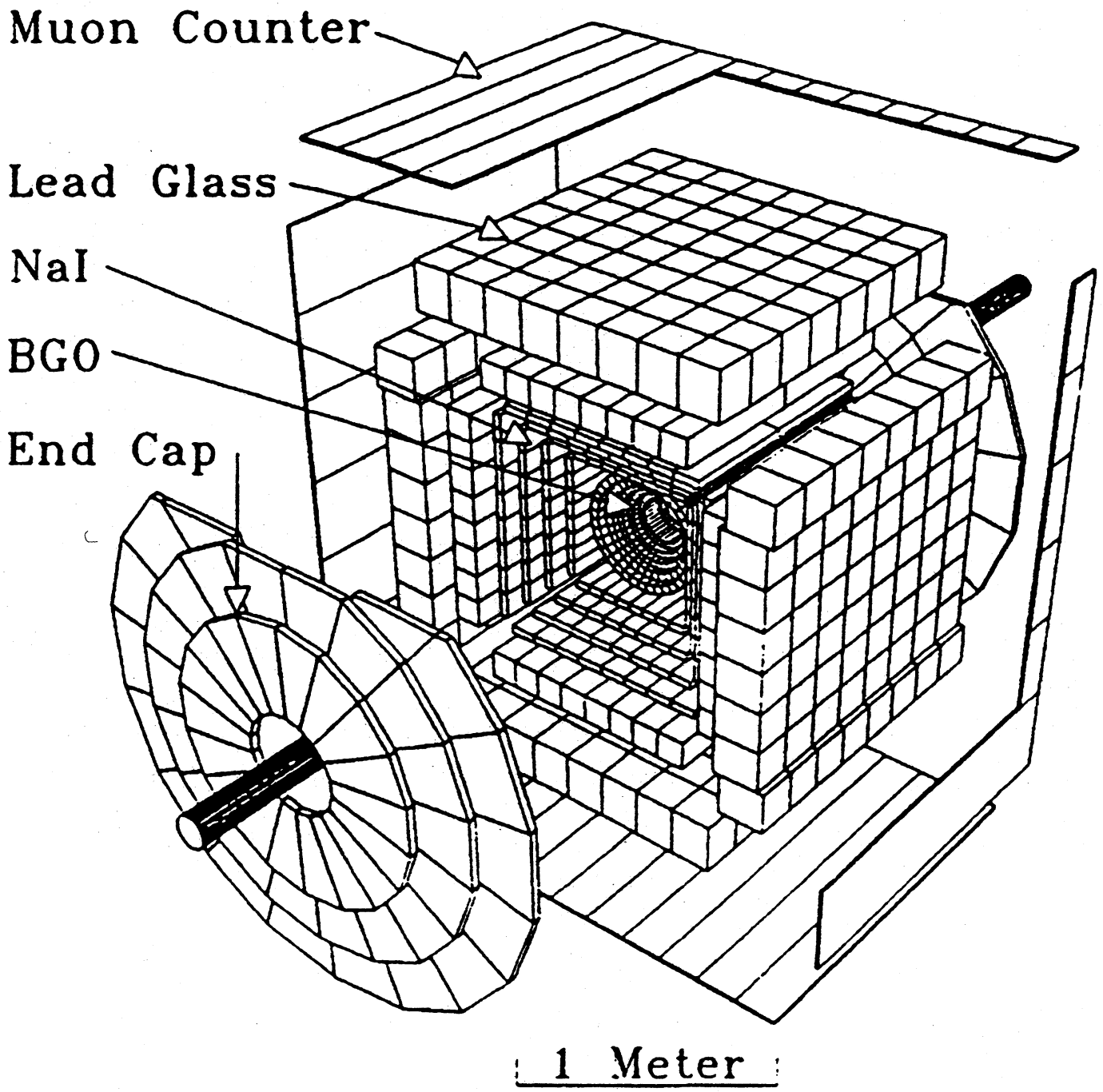
Muon Counter
Lead Glass
NaI
BGO
End Cap
1 Meter

Event Displays in CUSB-II: top-left: Bhabha, top-right: $\pi\pi\mu\mu$, bottom-left $\mu\mu\gamma\gamma$, bottom-right hadronic event

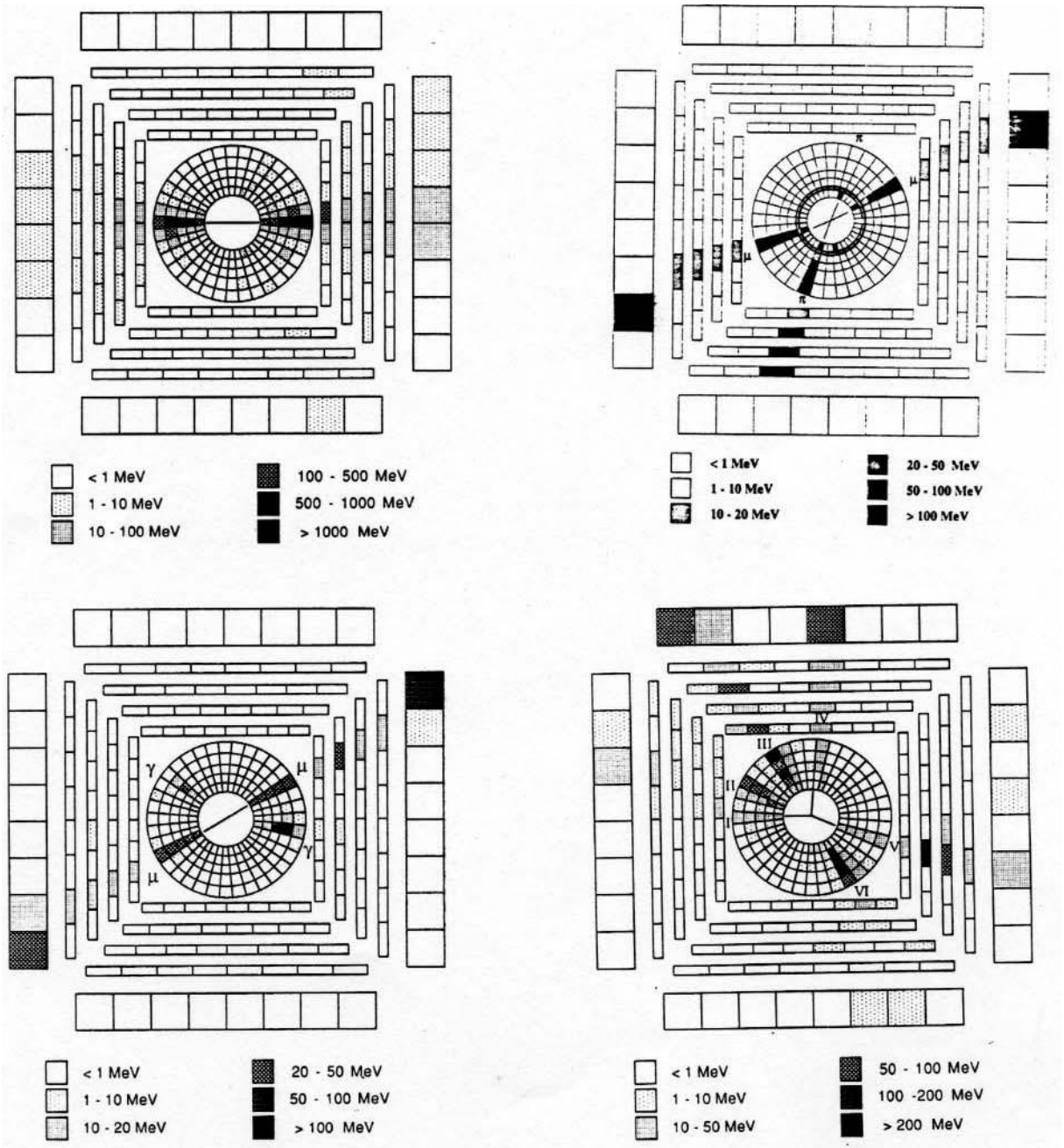

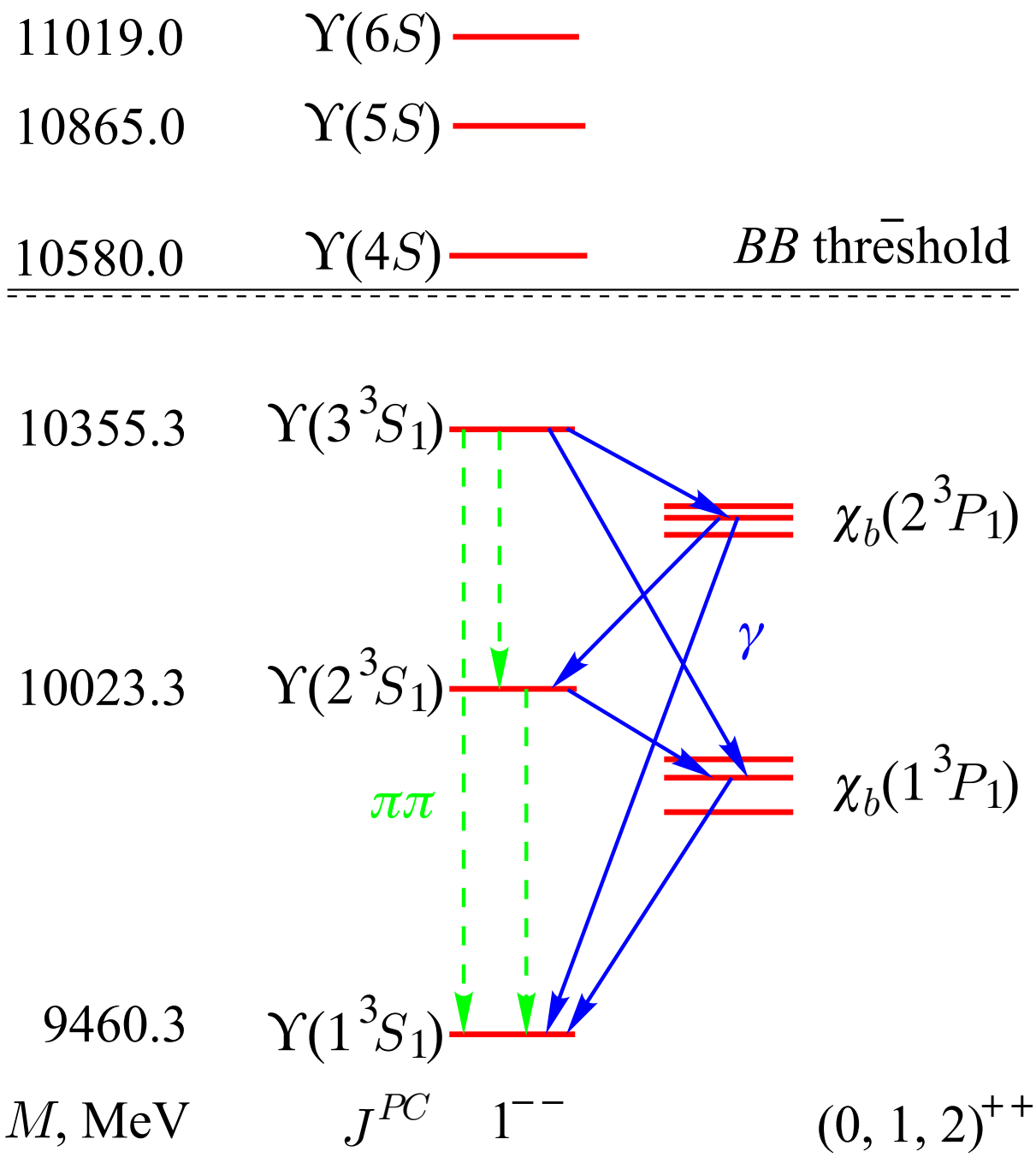
11019.0
$\Upsilon(6S)$
10865.0
$\Upsilon(5S)$
10580.0
$\Upsilon(4S)$
$B\bar{B}$ threshold
10355.3
$\Upsilon(3\,^3S_1)$
$\chi_b(2\,^3P_1)$
γ
10023.3
$\Upsilon(2\,^3S_1)$
$\pi\pi$
$\chi_b(1\,^3P_1)$
9460.3
$\Upsilon(1\,^3S_1)$
M, MeV
J^{PC}
1^{--}
$(0, 1, 2)^{++}$

Exclusive Decay from $\Upsilon(3S) \rightarrow \chi_b(2P_J) + \gamma \rightarrow \Upsilon(1S, 2S)\gamma\gamma$ and the Υ's annihilate into a pair of leptons. top-left:$3S \rightarrow 2P\gamma \rightarrow 1S\gamma$, central: $3S \rightarrow 2P\gamma \rightarrow 1S\gamma$, bottom: $3S \rightarrow 2P\gamma \rightarrow 2S\gamma$

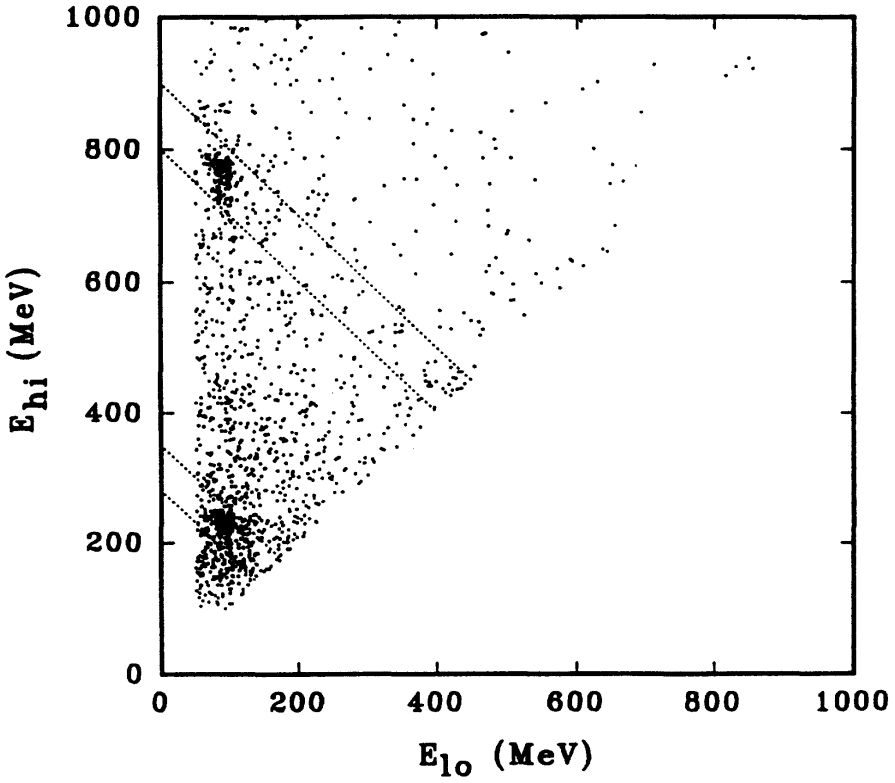

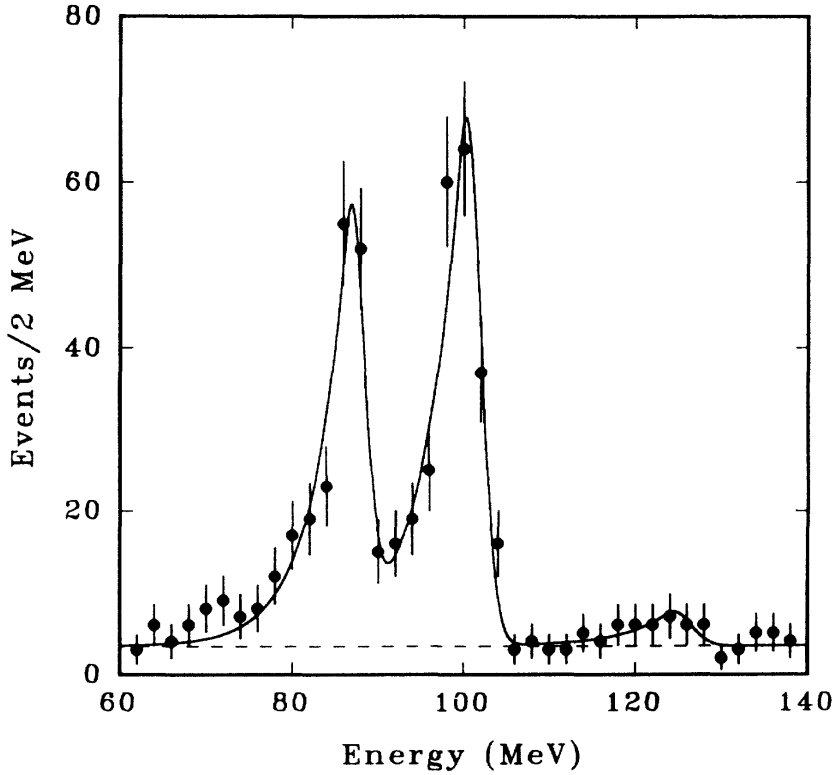

Inclusive Decay Spectrum from $\Upsilon(3S)$:(1) $3S \rightarrow 2P$(2)2P$\rightarrow$2S (4+5) $3S \rightarrow 1P, 1P \rightarrow 1S$ (3) $2P \rightarrow 1S$

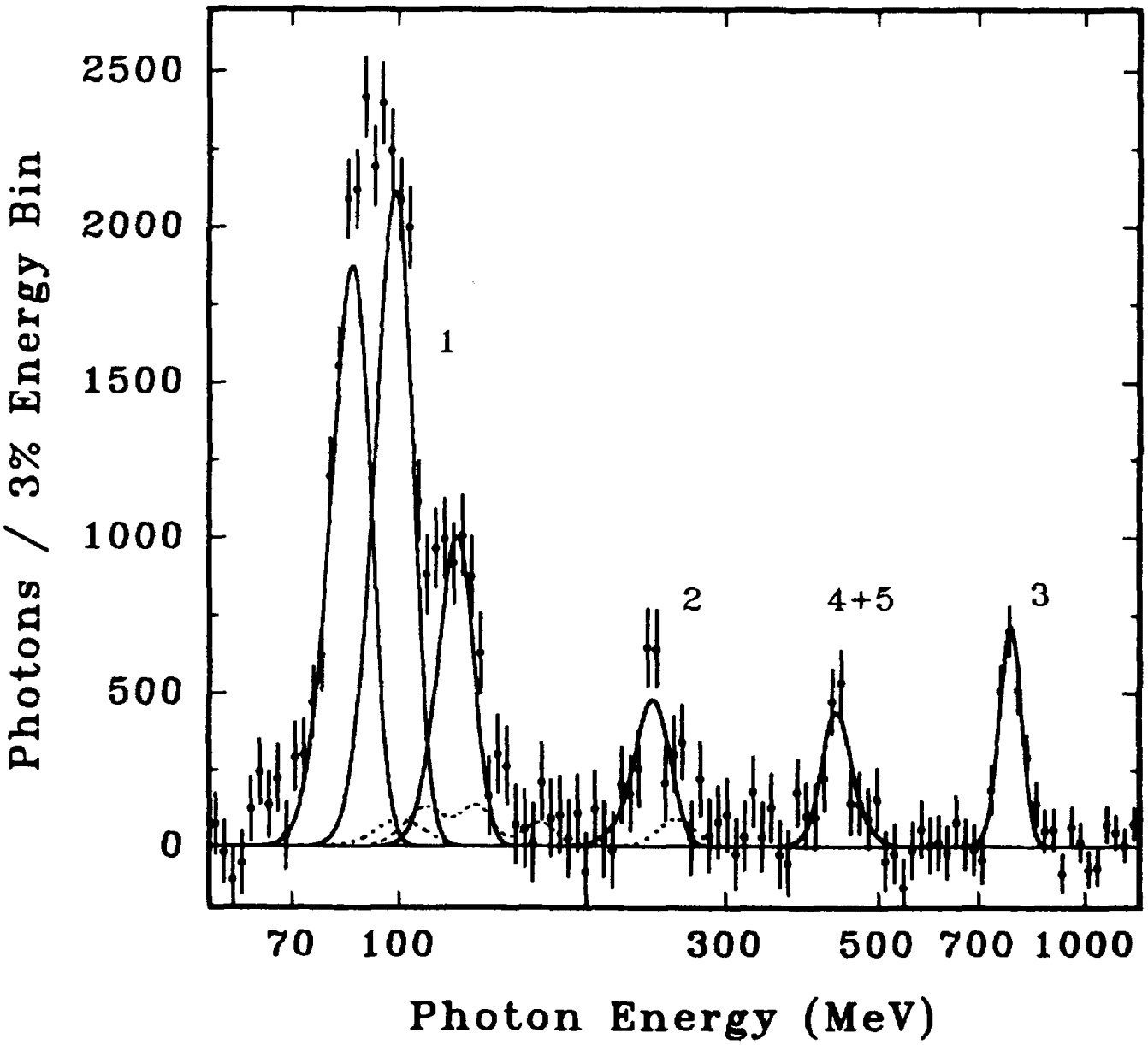

SPIN DEPENDENT INTERACTIONS

$$V(r) = \frac{1}{2m_Q^2 r}\ \vec{L}\cdot\vec{S}\ \ (3\mathrm{d}/\mathrm{d}rV_v - \mathrm{d}/\mathrm{d}rV_s)\ \ \text{spin}-\text{orbit}$$

$$+\frac{S_{12}}{12m_Q^2}\ \left(\frac{1}{r}\mathrm{d}/\mathrm{d}rV_v - \mathrm{d}^2/\mathrm{d}r^2V_v\right)\ \ \text{tensor}$$

$$+\frac{2}{3m_Q^2}\ \vec{S}_1\cdot\vec{S}_2\ \nabla^2 V_v\ \text{spin}-\text{spin},\ \ \text{vanishes for}\ L\neq 0$$

$$\text{with}\ S_{12} = 2\ (3\ \hat{r}\cdot\vec{S}_1\ \hat{r}\cdot\vec{S}_2 - \vec{S}_1\cdot\vec{S}_2)$$

$$V(r) = V_v + V_s.$$

$$V_s = A + Br, \qquad \text{and}\ V_v = -\frac{4}{3}\frac{\alpha_s}{r}$$

$$\langle\vec{L}\cdot\vec{S}\ \rangle = \ L,\ -1,\ -(L+1) \qquad \text{for}\ \ J\ =\ L+1,\ L,\ L-1.$$

this
is
tex

$$\langle S_{12} \rangle \;=\; -\frac{2L}{2L+3},\; 2,\; -\frac{2L+1}{2L-1} \quad \text{for} \quad J \;=\; L+1,\; L,\; L-1$$

$$M(\chi_b(2P_2)) = \overline{M} + a - \frac{2b}{5}$$
$$M(\chi_b(2P_1)) = \overline{M} - a + 2b$$
$$M(\chi_b(2P_0)) = \overline{M} - 2a - 4b,$$

where a and b are the expectation values of the spin-orbit and tensor pieces of the potential:

$$a = \frac{1}{2m_Q^2}\left\langle \frac{3V_v'}{r} - \frac{V_s'}{r} \right\rangle$$
$$b = \frac{1}{12m_Q^2}\left\langle \frac{V_v'}{r} - V_v'' \right\rangle .$$

We have determined the branching ratios of ($\Upsilon'' \to \chi_b(2P_{2,1,0})\gamma$), product branching ratios of ($\Upsilon'' \to \chi'(2P_{2,1,0})\gamma \to \Upsilon'\gamma\gamma$), of ($\Upsilon'' \to \chi_b(2P_{2,1,0})\gamma \to \Upsilon\gamma\gamma$) and precision measurements of the electric dipole transition rates from Υ'' to χ'.

We have measured the center of gravity of the $\chi_b(2P)$ states to be (10259.5±0.4±1.0), which Christine Davies's Lattice QCD calculations has confirmed.

The fine structure splittings obtained using our data are $M(\chi_2') - M(\chi_1') = 13.5 \pm 0.5$ MeV, and $M(\chi_1') - M(\chi_0') = 23.2 \pm 1.0$ MeV.

These in turn determine the spin orbit a=9.5±0.22 MeV and the tensor interaction b=2.3±0.14 MeV.

Fine structure of the χ_b' state
resolved in their spin-orbit and tensor contributions
as determined by CUSB. Energies are in MeV.

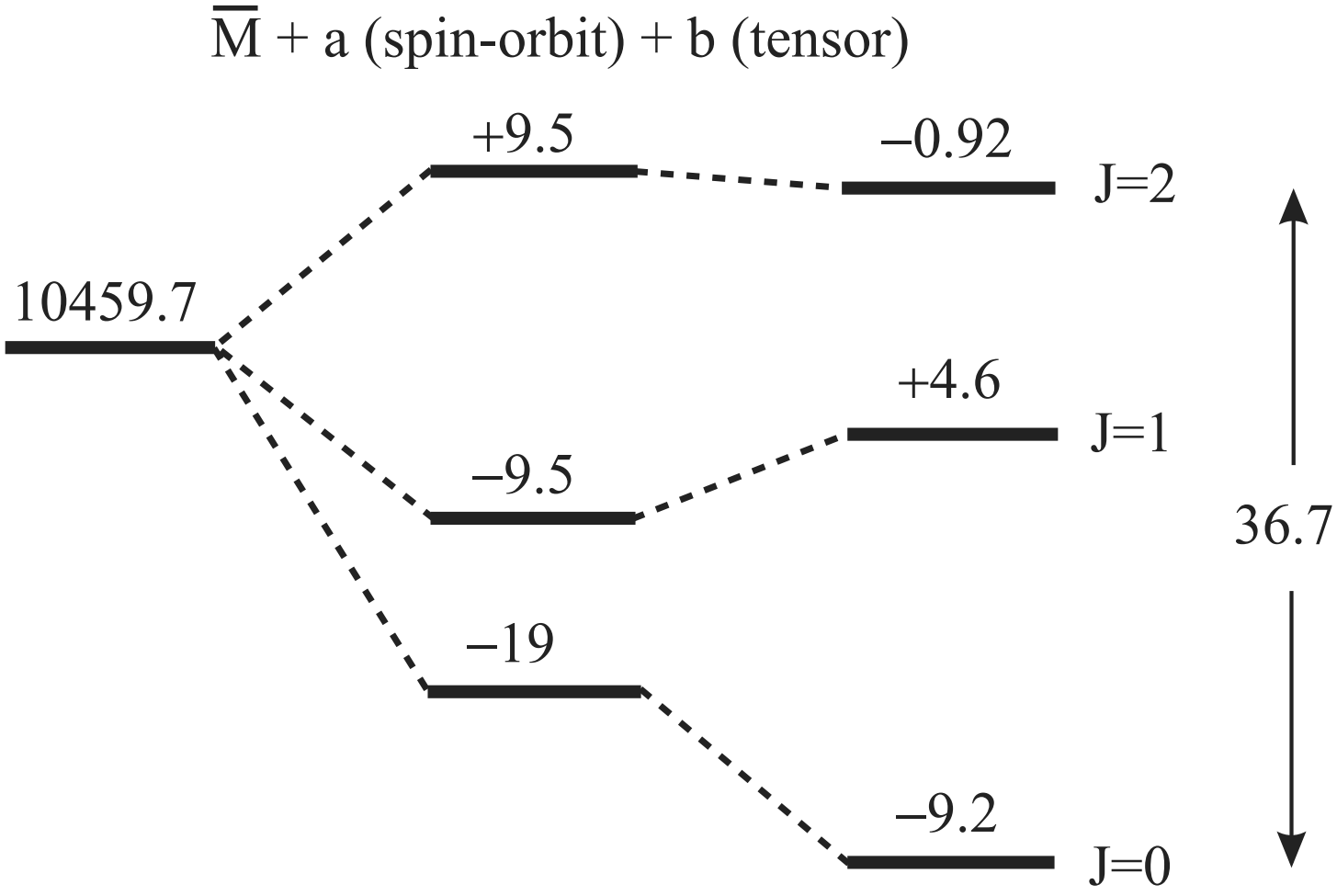

The above results confirm expectations that the long range, confining part of the quark anti-quark potential is due to the exchange of an effective (multi-gluon) scalar state (a flux tube),
while the short range, coulombic part is due to single gluon (vector) exchange.
We also used our fine structure measurements to quantitatively determine f defined as the coefficient which multiplies kr in the spin dependent potential $(V_v + V_s)$.
Using the value of the string tension k which is presently known to be between 0.14 and 0.18 GeV^2, we obtained that $f \sim 1$ with an error of about 5%.

We measured the $\pi\pi$ transitions between the Υ states.

looking at the Feymann diagrams for such transitions: Amplitudes for :(a) electric dipole transitions (E1) $^3S(^3P) \rightarrow ^3 P(^3S) + \gamma$

(b) double color-electric dipole transitions $n^3S \rightarrow (n-1)^3S + gg(2\pi)$.

we expected the dipion spectra to be similar to that given by electric dipole transitions.

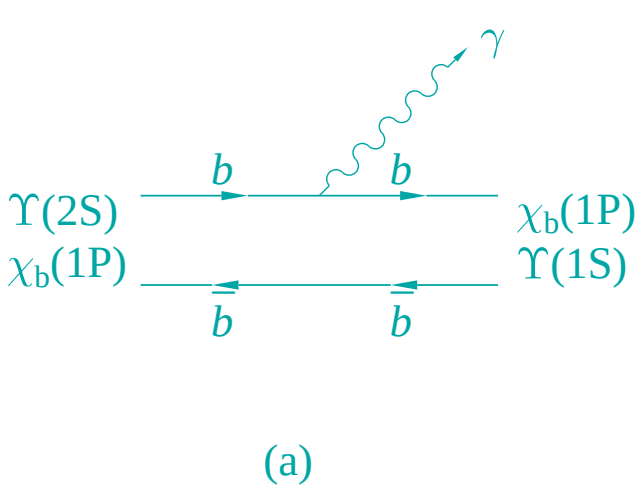

(a)

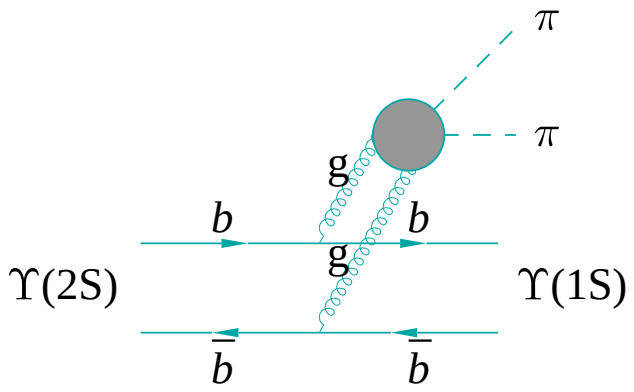

(b)

This was found to be correct in the $\pi\pi$ transitions from the $\Upsilon(3S, 2S)$ to $\Upsilon(2S, 1S)$ ground state. In addition, the fact that the branching ratio of the $\pi^+\pi^-$ is twice that of the $\pi^0\pi^0$ channel means the dipions have Isospin 0, that these transitions have ΔI =0, thus verify the Υ's are Isospin singlets.

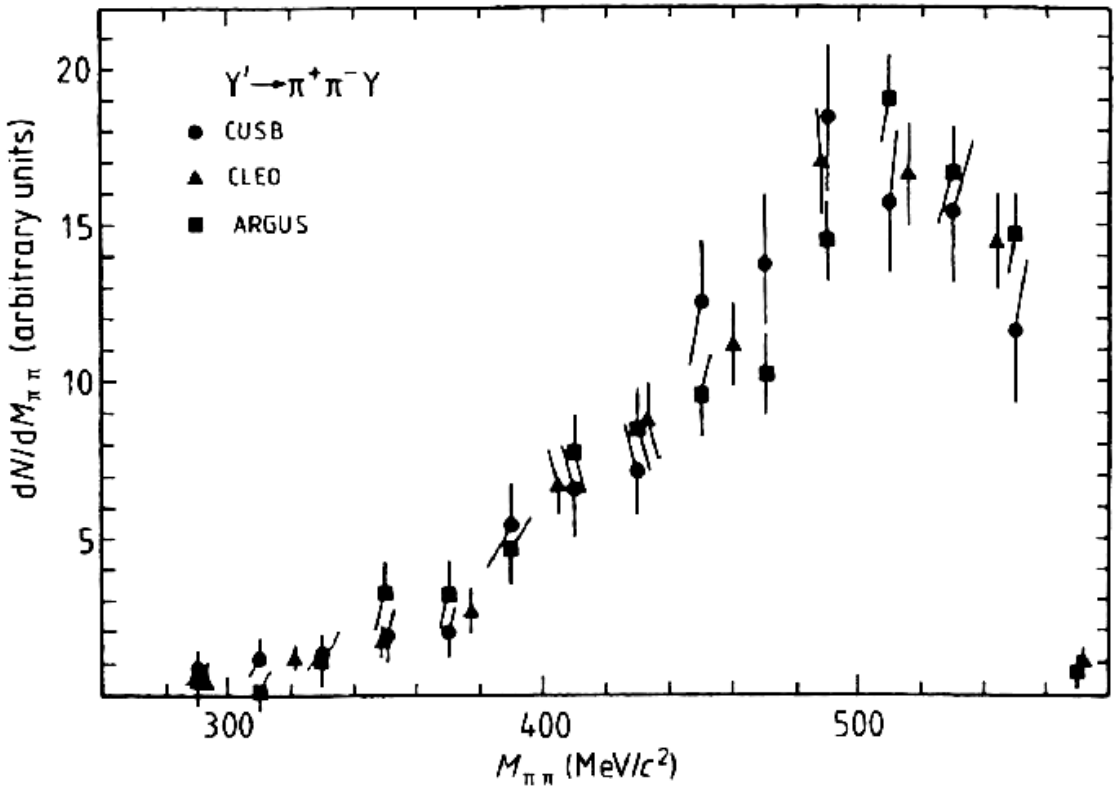

However, the dipion mass spectrum from the $\Upsilon(3S) \rightarrow \Upsilon(1S)$ has a two humped structure that no theoretical model has been able to reproduce, shown below.

It is nice that 12 years later CLEO-III has confirmed this anomaly.

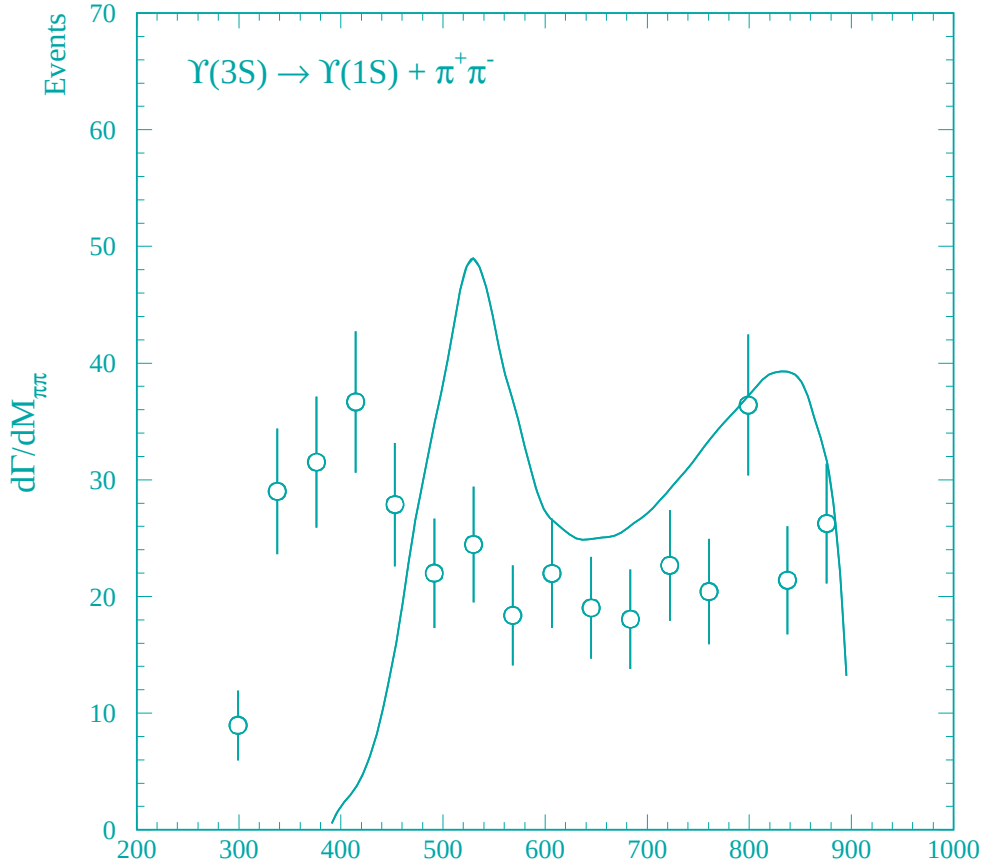

HIGGS, GLUINOS, SQUARKS to SBOTTOMONIUM

We have performed many null result searches using our photon spectra. An interesting new note is that they have been used in 2002 to set limits on sbottomnium by BERGER.

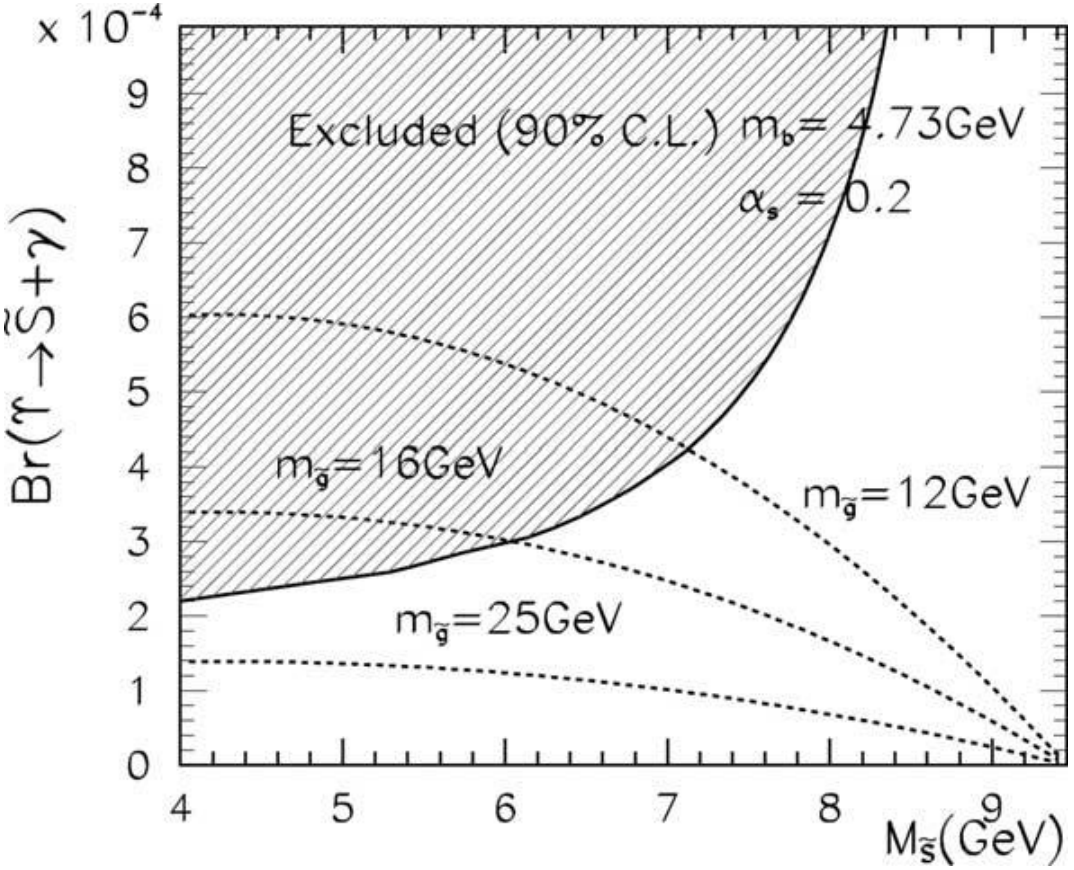

Fig. 2. Branching fraction for the process S as a function of M S. The shaded area is excluded at the 90% confidence level by the X search of the CUSB Collaboration [11].

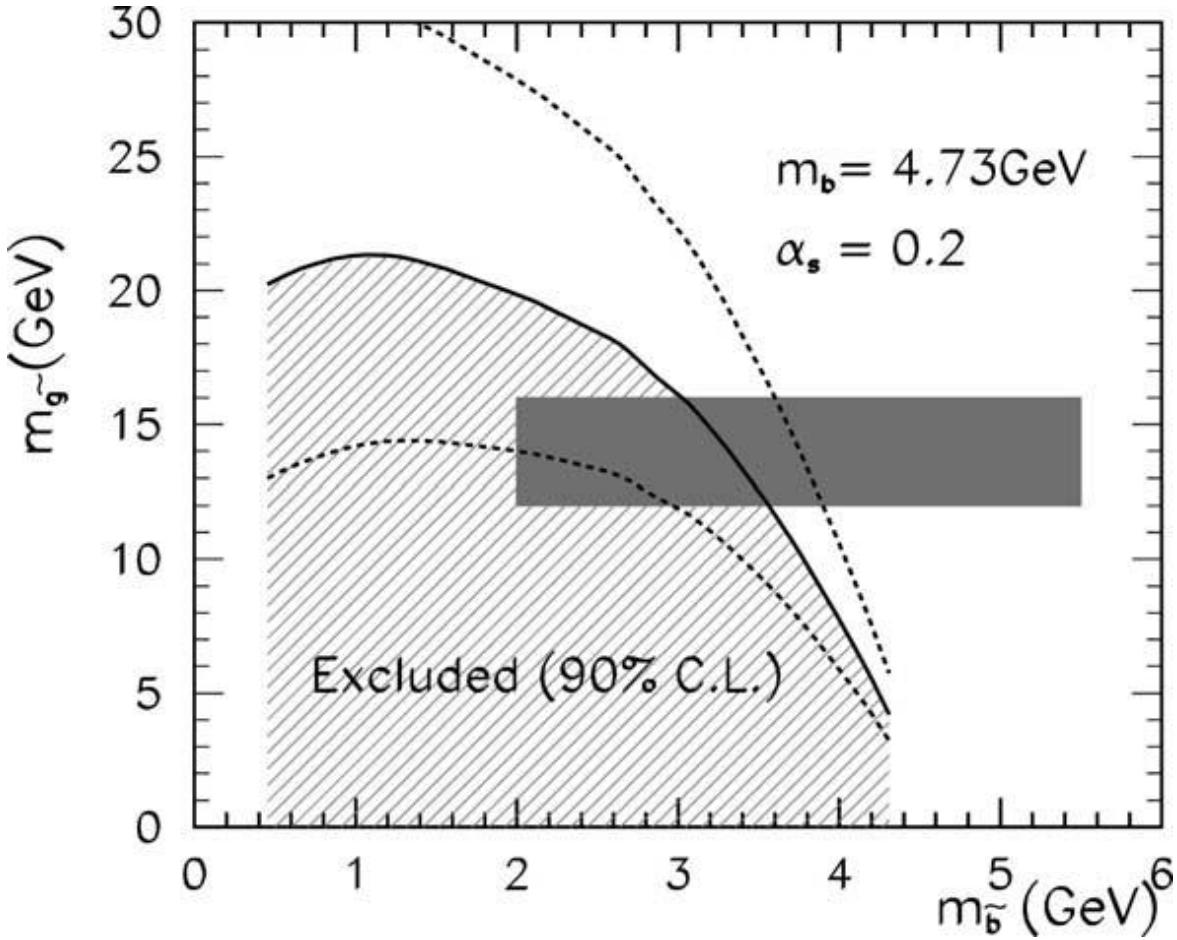

Fig. 3. The regions of the $m_{\tilde{b}}$–$m_{\tilde{g}}$ parameter space that are excluded at the 90% confidence level by the X search of the CUSB Collaboration (shaded region) [11]. The solid curve represents the central value of the theoretical calculation, and the dashed curves show the uncertainties on the theoretical values, as described in the text. The strip shows the region $2 < m_{\tilde{b}} < 5.5$ GeV, $12 < m_{\tilde{g}} < 16$ GeV proposed in the light-bottom-squark scenario [3].

this
is
tex

KLOE: A SAMPLING CALORIMETER enclosing a drift chamber.

The KLOE detector

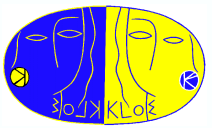

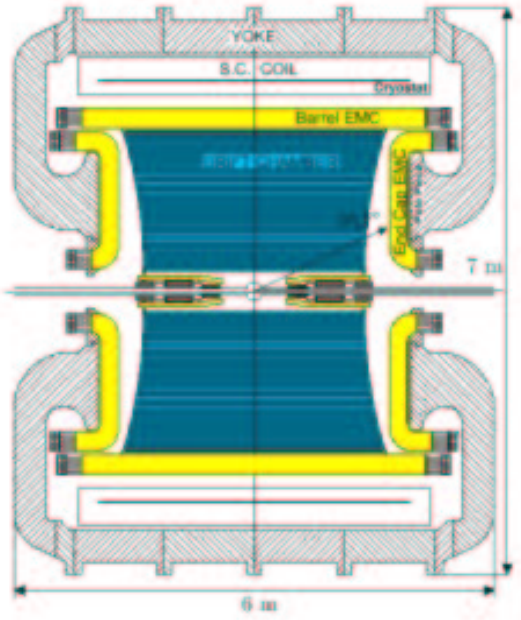

- **Drift chamber:**
  Large volume d=4m l=3.3m
  He – iC_4H_{10} 90%-10% gas mixt.
  Momentum resolution : $\delta p/p < 0.4\%$
  Sp. resol.: $\sigma_{xy} \approx 150\ \mu m$; $\sigma_z \approx 2$ mm
- **E.m. calorimeter:**
  Sampling calorimeter: Pb-scintillating fibres
  Energy resolution: $\sigma_E/E = 5.4\% / \sqrt{(E(GeV))}$
  Time resolution:
  $\sigma_t = 55$ ps $/ \sqrt{(E(GeV))} \oplus 40$ ps (cal.) $\oplus 120$ ps (coll.time)
  Read-out granularity: 4.4×4.4 cm^2
  Acceptance: 98% of 4π
- **Magnetic field:** 0.53 T

The calorimeter of made of grooved lead layers rolled out from a spaghetti machine, into whose grooves 1mm scintillating fibers are laid. The lead to scintillating fibers ratio is such that the lead is not even visible to the naked eye.

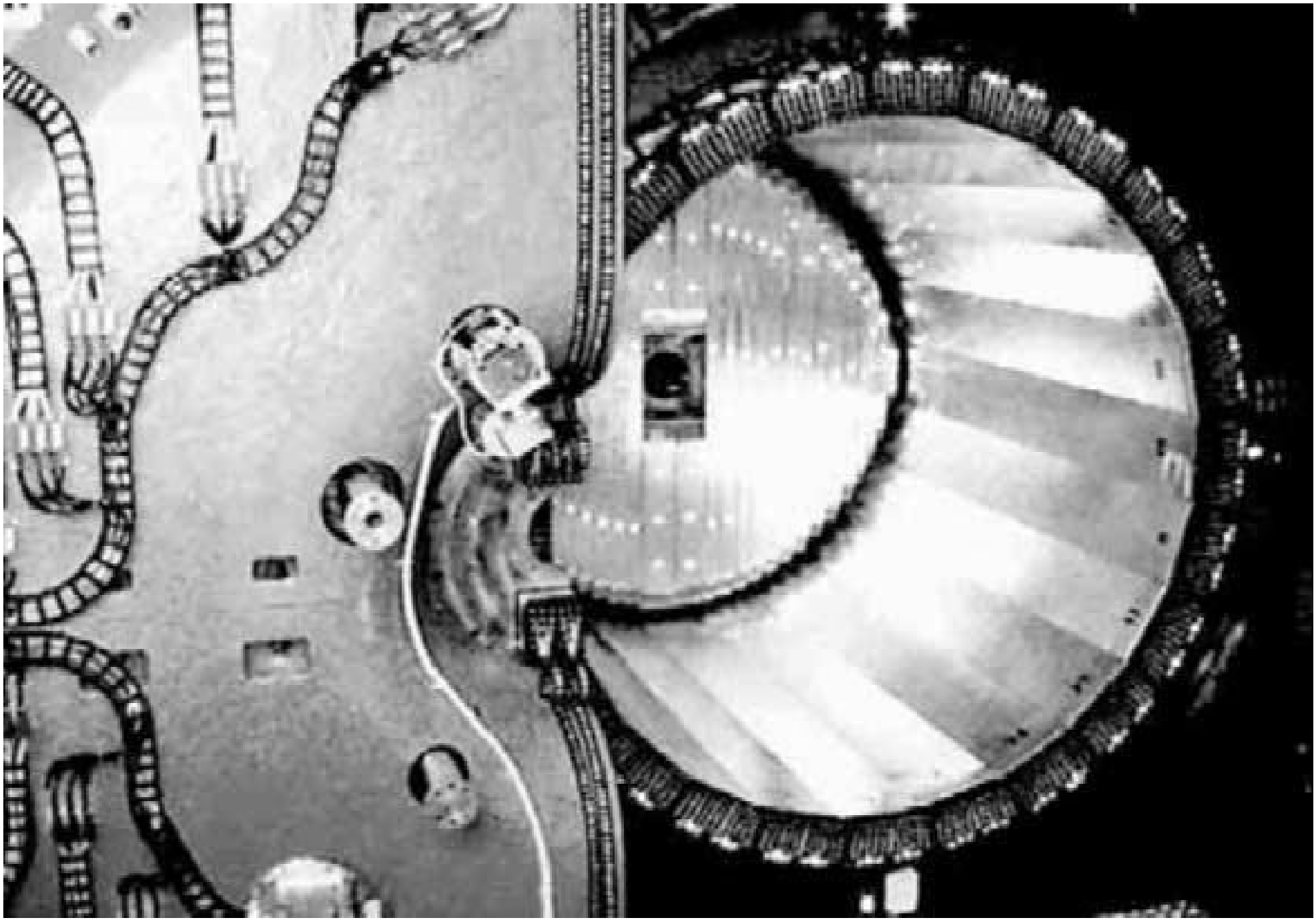

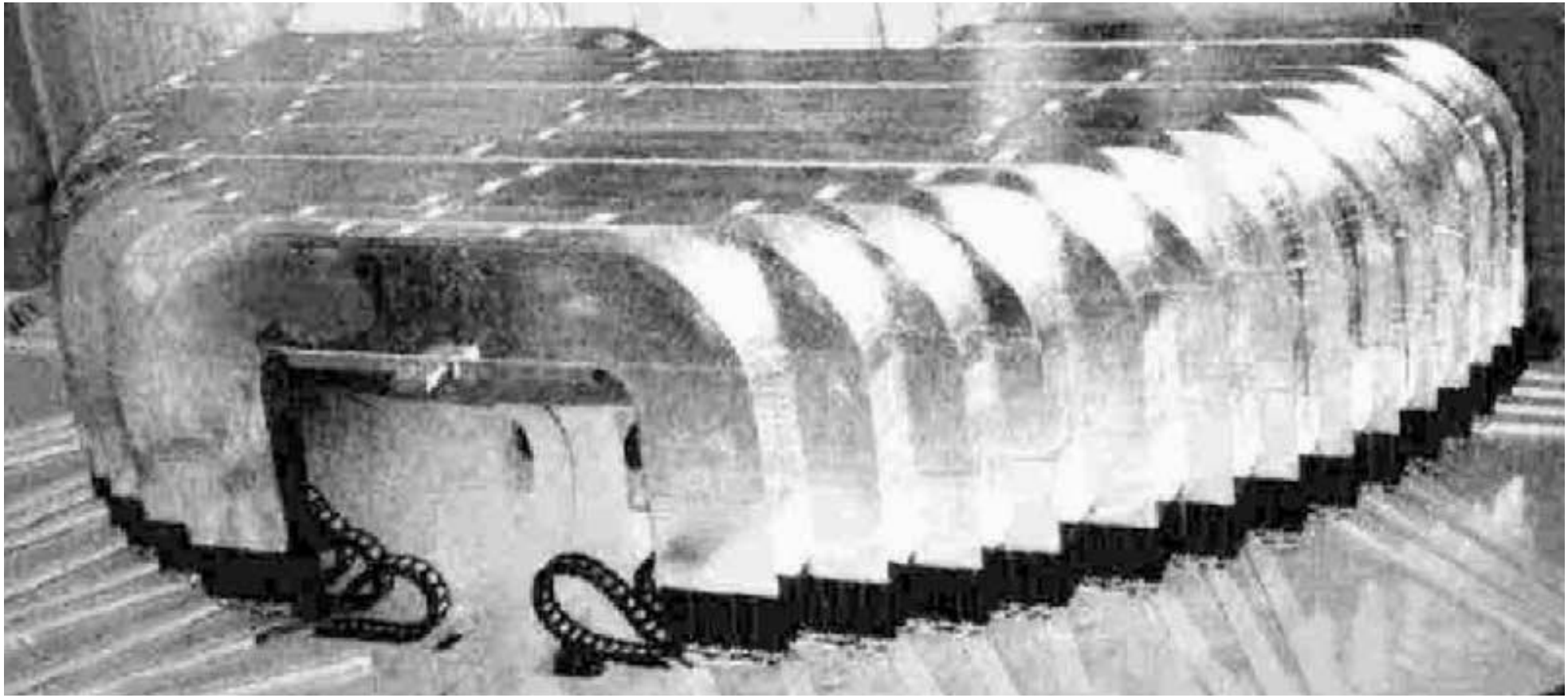

Light Quark Spectroscopy

In a previous lecture by Paolo he described the octets of hadrons as a kind of mathematical construct, ignoring the mechanism for the binding of the light quarks into the hadrons.

Of course the force responsible is QCD, but what is the shape of the color potential? Coulombic as in QED? Linear as in a color tube? As we have seen a superposition of the two as had been proved for heavy quark systems.

Lattice QCD

Flux tubes realized

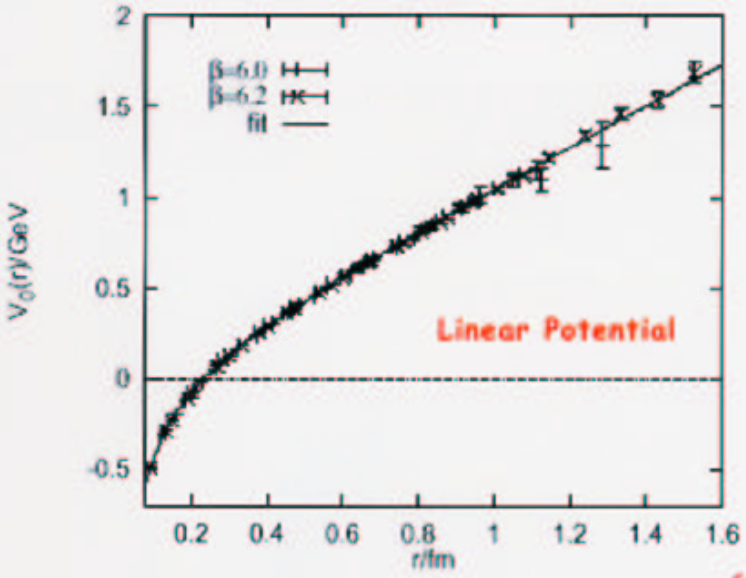

from Bali et al

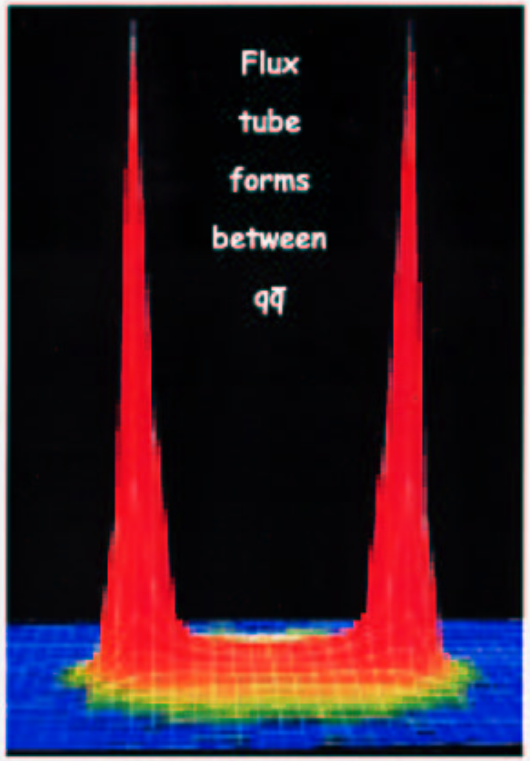

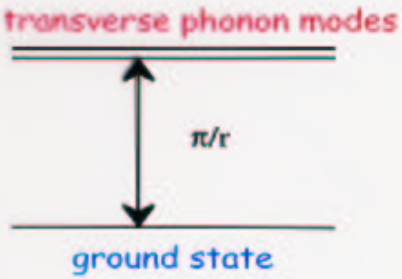

1. Confinement arises from flux tubes.
2. The excitation of these flux tubes leads to a new spectrum of mesons.

this
is
tex

The way we can get an answer is to assume a potential, solve the Schroedinger's equation, obtain a spectra or a level diagram and try to see whether we can fill these diagrams with particles whose quantum numbers we have determined, for ex:

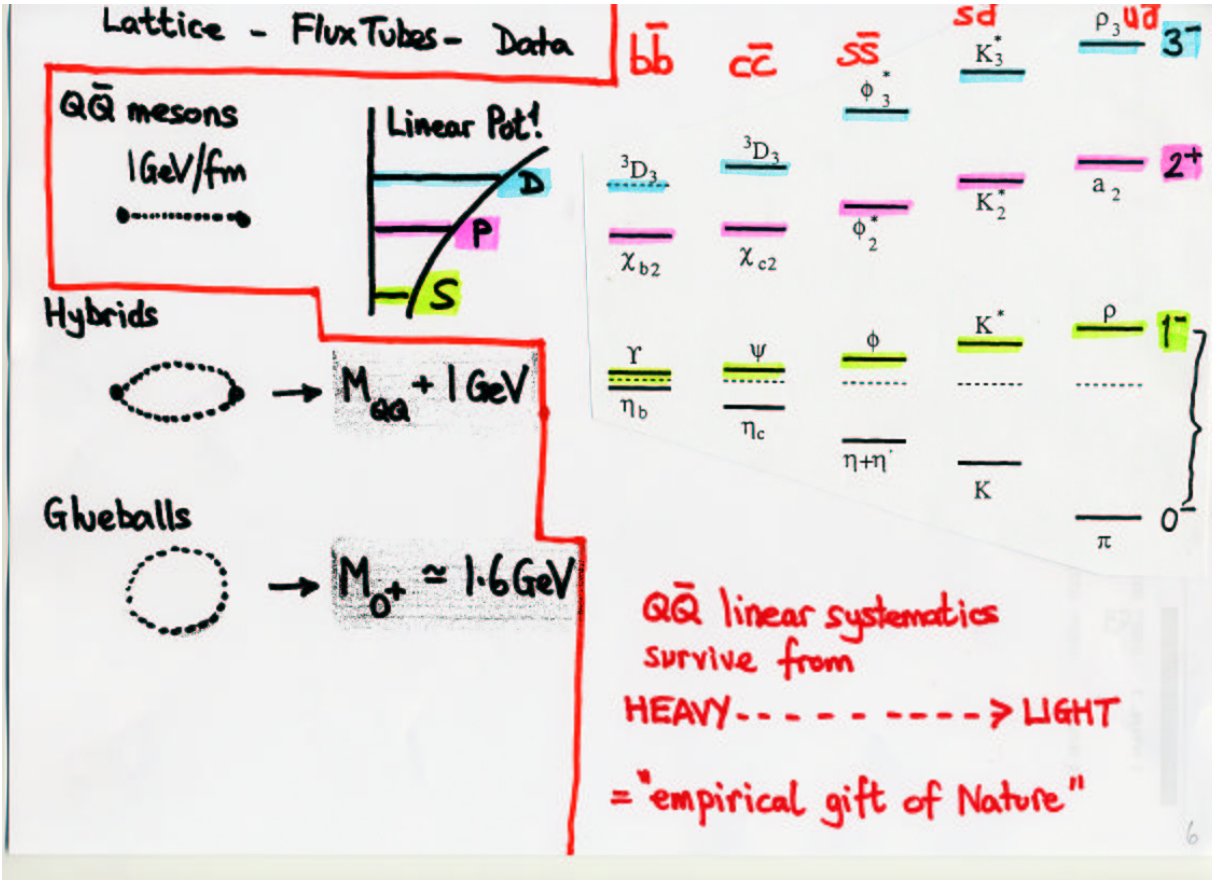

On the other hand, Jaffe long ago had pointed out that there is a strong QCD attraction among qq and $\bar{q}\bar{q}$ in S wave, 0^{++}, it is as if they are confined in a "bag", a spherical potential, $V(r) \sim \lambda r^u$.

Credence to this possibility was enhanced by Isgur and Weinstein motivating an attraction between such mesons if they could be interpreted as $Q\bar{Q}$ molecules. The most interesting difference between the spherical and the linear potential is the inversion of the mass spectra of the states.

Furthermore, the coupling constants between the states and the constituents are different.

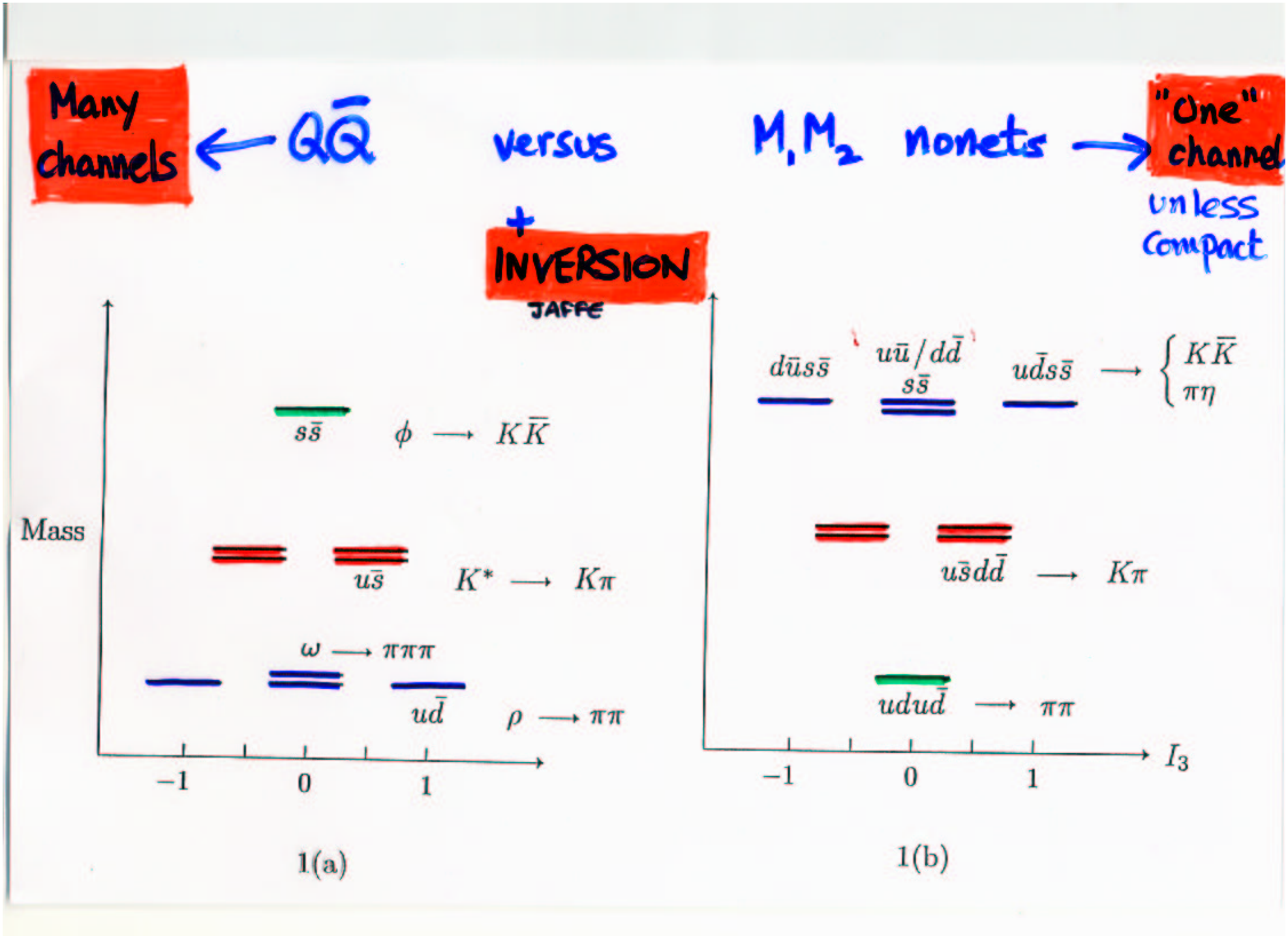
Many channels
← QQ̄ versus M1M2 nonets →
"One" channel
unless Compact
+
INVERSION
JAFFE
Mass
ss̄
φ → KK̄
us̄
K* → Kπ
ω → πππ
ud̄
ρ → ππ
−1
0
1
1(a)
dūss̄
uū / dd̄
ss̄
ud̄ss̄
→ KK̄
πη
us̄dd̄
→ Kπ
udud̄
→ ππ
I3
−1
0
1
1(b)

As resonances have been found one after another, they fit well in the $q\bar{q}$ spectrum, except in the 1 GeV region where we seem to have an excess of an isosinglet, f_0 and an isotriplet a_0 of scalars left over. Their nature are a puzzle debated now for many many years.

Frank Close in 2001 points out that below the 1 GeV region, near the $K\bar{K}$ threshold, is where the JAFFE-ISGUR S-wave binding is expected to dominate over the P-wave $q\bar{q}$ formation.

In 2001 KLOE had collected the largest number collected at that time of $f0$'s and $a0$'s. In the following I show our first determinations of the BR's and coupling constants.

$\phi \to S(0^{++})\gamma$

- **S = $f_0(980)$ (I=0) , $a_0(980)$ (I=1) are not easily interpreted as $q\bar{q}$ states**
- **Other possible interpretations: $q\bar{q}q\bar{q}$ states**
  $K\bar{K}$ molecules
- **Br($\phi \to f_0(980)\gamma$) and Br($\phi \to a_0(980)\gamma$) are sensitive to the nature of these scalar particles**

- **$\phi \to f_0\gamma$; $f_0 \to \pi^0\pi^0$ 5 γ final state**
  ($f_0 \to \pi^+\pi^-$ large background from Initial State Radiation and Final State Radiation (interference))
- **$\phi \to a_0\gamma$; $a_0 \to \eta\pi^0$ $\eta \to \gamma\gamma$ (39%) 5 γ final state**
  " " $\eta \to \pi^+\pi^-\pi^0$ (23%) 2 tracks +5 γ
  first observation
  ($\eta \to \pi^0\pi^0\pi^0$ (32%) 9 γ final state)
- **Data sample : 16 pb^{-1} from the 2000 data**

Model

- **Scalar term: (S=f_0,σ)**

$$A_{S\gamma}(m) = \frac{2m^2}{\pi} \frac{\Gamma_{\varphi S\gamma}\Gamma_{S\pi^0\pi^0}}{|D_s|^2} \frac{1}{\Gamma_\varphi} \quad ; \quad m = M_{\pi\pi}$$

- **f_0 term from kaon loop : (Achasov-Ivanchenko,** Nucl.Phys.B315(1989)465)

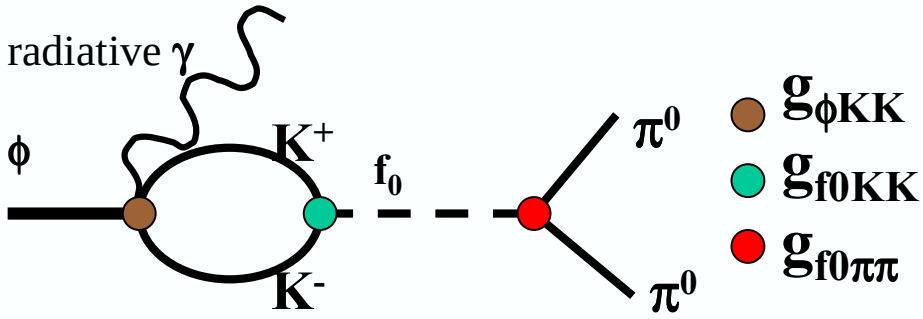

$$\Gamma_{\varphi f_0\gamma}(m) = \frac{g^2_{f_0K^+K^-} g^2_{\varphi K^+K^-}}{12\pi} \frac{|g(m)|^2}{M_\varphi^2} \left(\frac{M_\varphi^2 - m^2}{2M_\varphi} \right)$$

$$g_{\varphi K^+K^-} = 4.68 \quad \text{from } \Gamma(\varphi \to K^+K^-)$$

Model

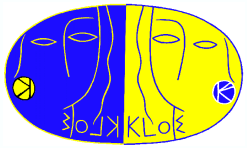

• σ term (Gokalp,Yilmaz, Phys.Rev.D64(2001)053017)

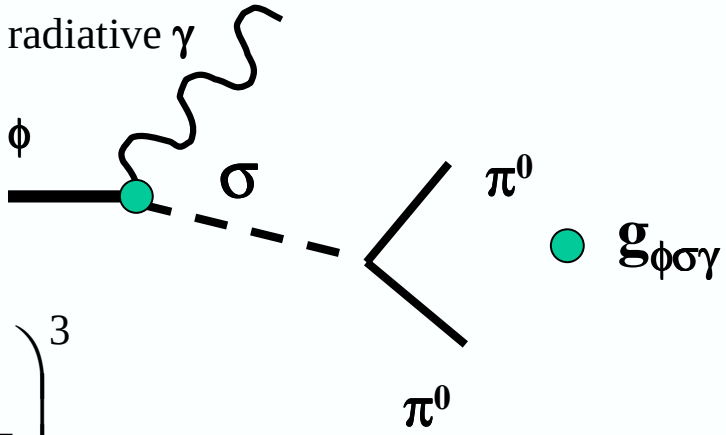

$$\Gamma_{\varphi\sigma\gamma}(m) = \frac{e^2 g^2_{\varphi\sigma\gamma}}{12\pi}\frac{1}{M^2_\varphi}\left(\frac{M^2_\varphi - m^2}{2M_\varphi}\right)^3$$

• **Decay width:** $\Gamma_{S\pi^0\pi^0}(m) = \frac{1}{2}\Gamma_{S\pi^+\pi^-}(m) = \frac{g^2_{S\pi^+\pi^-}}{32\pi m}\sqrt{1-\frac{4M^2_\pi}{m^2}}$

• **Inverse propagators: D_{f0} with finite width corrections, from Achasov-Ivanchenko,** Nucl.Phys.B315(1989)465

D_σ = Breit-Wigner with M_σ=478 MeV and Γ_σ=324 MeV (Fermilab E791-Phys.Rev.Lett.86(2001)770)

• **ρπ + interference term parameterizations from Achasov-Gubin,** Phys.Rev.D63(2001)094007

this is tex

Fit results

- Large f_0-σ destructive interference at $M_{\pi\pi} < 700$ MeV

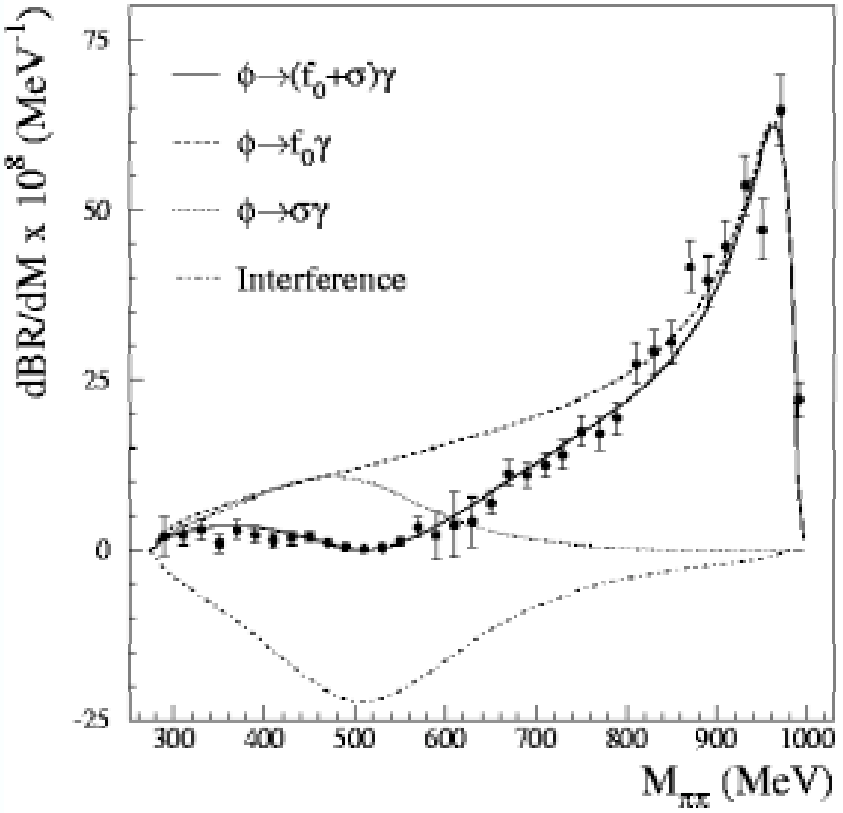

- By integrating over the f_0 and σ curves:

$Br(\phi\to f_0\gamma\to\pi^0\pi^0\gamma) = (1.49 \pm 0.07) \times 10^{-4}$

$Br(\phi\to\sigma\gamma\to\pi^0\pi^0\gamma) = (0.28 \pm 0.04) \times 10^{-4}$

this is tex

Fit results

χ^2/ndf	27.2/25
$g^2_{a0KK}/(4\pi)$ (GeV^2)	0.40 ± 0.04
$g_{a0\eta\pi}/g_{a0KK}$	1.35 ± 0.09
$Br(\phi \to \rho^0\pi^0 \to \eta\pi^0\gamma)$	$(0.5 \pm 0.5) \times 10^{-5}$

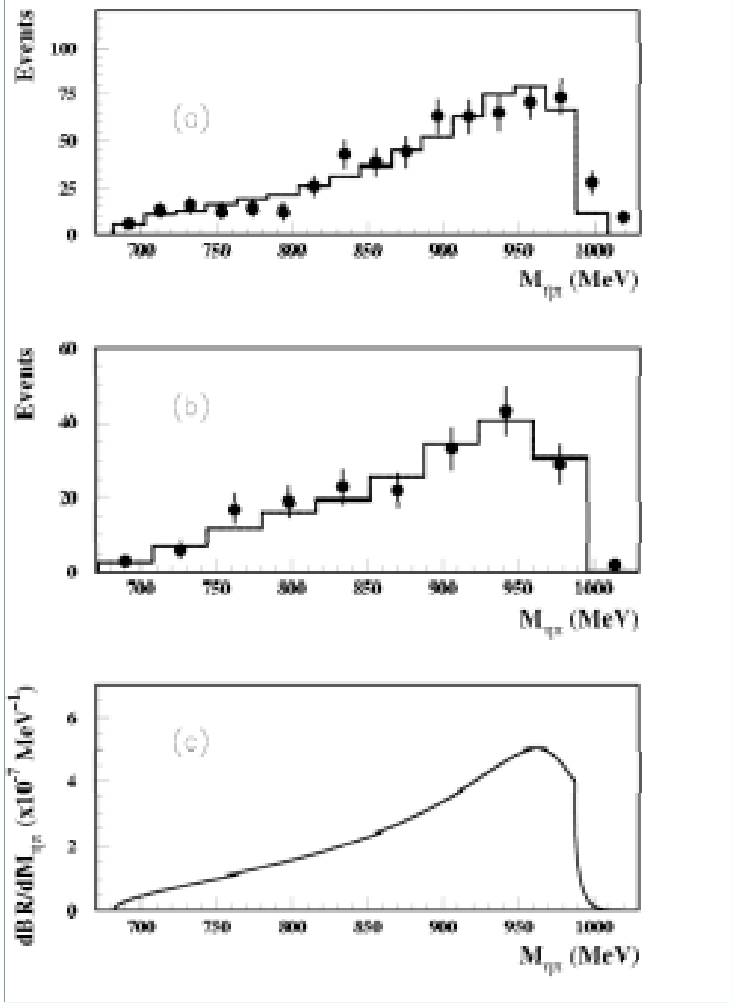

- By integrating over the whole spectrum:

$Br(\phi \to a_0\gamma \to \eta\pi^0\gamma) = (7.4 \pm 0.7) \times 10^{-5}$

this
is
tex

Summary of couplings

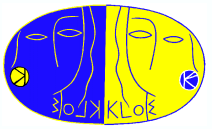

- Comparison with predictions based on the kaon loop model with point-like coupling of the scalars to kaons (Achasov-Ivanchenko)

	KLOE	qqqq	$qq^{(1)}$	$qq^{(2)}$
$g^2_{f0KK}/(4\pi)$ (GeV^2)	2.79±0.12	"super-allowed" (~2 GeV^2)	"OZI-allowed"	"OZI-forbidden"
$g_{f0\pi\pi}/g_{f0KK}$	0.50±0.01	0.3—0.5	0.5	2
$g^2_{a0KK}/(4\pi)$ (GeV^2)	0.40±0.04	"super-allowed" (~2 GeV^2)	"OZI-forbidden"	"OZI-forbidden"
$g_{a0\eta\pi}/g_{a0KK}$	1.35±0.09	0.91	1.53	1.53

(1) $f_0 = s\bar{s}$; $a_0 = (u\bar{u} - d\bar{d})/\sqrt{2}$

(2) $f_0 = (u\bar{u} + d\bar{d})/\sqrt{2}$; $a_0 = (u\bar{u} - d\bar{d})/\sqrt{2}$

- f_0 parameters are compatible with qqqq model
- a_0 parameters seem not compatible with qqqq model

KEEP POSTED FOR NEWS IN 2003!! 25 × STATISTICS!

this is tex